DELAYED TRIGGERING OF EARLY AFTERSHOCKS BY MULTIPLE SURFACE WAVES CIRCLING THE EARTH

A Thesis
Presented to
The Academic Faculty

by

Brendan Sullivan

In Partial Fulfillment
of the Requirements for the Degree
Master of Science in the
School of Earth and Atmospheric Sciences

Georgia Institute of Technology
December 2012

DELAYED TRIGGERING OF EARLY AFTERSHOCKS BY MULTIPLE SURFACE WAVES CIRCLING THE EARTH

Approved by:

Dr. Zhigang Peng, Advisor
School of Earth and Atmospheric Sciences
Georgia Institute of Technology

Dr. Andrew V. Newman
School of Earth and Atmospheric Sciences
Georgia Institute of Technology

Dr. Christian Huber
School of Earth and Atmospheric Sciences
Georgia Institute of Technology

Date Approved: August 24, 2012

ACKNOWLEDGEMENTS

I would like to thank my advisor Dr. Zhigang Peng for his guidance, patience and faith in me. I also thank my thesis committee members, Dr. Andrew Newman and Dr. Chris Huber, for reading this tome and providing helpful suggestions and commentary. I am also appreciative of the data, code and suggestions provided by Dr. Bogdan Enescu, Dr. Olivier Lengline, Dr. Andrew Michaels, Dr. Rick Aster, Dr. Karen Felzer, and Dr. Jiancang Zhuang. Also, my gratitude to Dr. Kurt Frankel, may he rest in peace, for rekindling my love of rocks. I would also like to thank the geophysics faculty, including Dr. Dufek, Dr. Paty and Dr. Wray for taking a chance on a non-traditional student. Thank you to all of the other grad students (and post docs), for their suggestions and encouragement (in no particular order)-- Christine, Chris J., Zach, Andy F., Jaime, Dr. Kevin, Chastity, Greg, Yan, Ash, Dr. Lujia, Josh, Joe, and the rest of the crew. Thank you to the many people who comprise the Community Online Resource for Statistical Seismicity Analysis for providing such wonderful and insightful tutorials and tools.

Finally, a warm thank you to my friends and family for being there for me during a difficult time. Too many to list. Luckily, you all will probably never read this, but I will make sure to tell you all about it...

TABLE OF CONTENTS

LIST OF TABLES

LIST OF FIGURES

SUMMARY

It is well known that direct surface waves of large earthquakes are capable of triggering shallow earthquakes and deep tremor at long-range distances. Recent studies have shown that multiple surface waves circling the earth could also remotely trigger microearthquakes. However, it is still not clear whether multiple surface waves returning back to the main shock epicenters could also trigger/modulate aftershock behavior. Here we conduct a study to search for evidence of such triggering by systematically examining aftershock patterns of earthquakes with magnitude ≥ 8 since 1990 that produce observable surface waves circling the globe repeatedly. We specifically examine the 2011 M9 Tohoku-Oki event using a composite catalog of JMA, HiNet and newly detected events obtained by waveform cross correlation. We compute the magnitude of completeness for each sequence, and stack all the sequences together to compute the seismicity and moment rates by sliding data windows. The sequences are also shuffled randomly and these rates are compared to the actual data as well as synthetic aftershock sequences to estimate the statistical significance of the results. Our results suggest that there is some moderate increase of early aftershock activity after a few hours when the surface waves return to the epicentral region. However, we could not completely rule out the possibility that such an increase is purely due to random fluctuations of aftershocks or caused by missing aftershocks in the first few hours after the mainshock.

CHAPTER 1

INTRODUCTION

1.1. Overview

Current observational evidence suggests that large earthquakes can dynamically trigger and modulate seismic activity at thousands of kilometers distance. To date, much research has focused on the triggering of microearthquakes in geothermal/volcanic systems or deep tectonic tremor along major plate boundary faults [Hill and Prejean, 2007; Peng and Gomberg, 2010]. However, recent studies have found that multiple surface waves traveling around the Earth several times could also trigger microearthquakes or deep non-volcanic tremor [Peng et al., 2011b; Zigone et al., 2012; Jay et al., 2012]. Surface waves sample the Earth's lithosphere and upper-mantle due to their long wavelengths, and are affected by heterogeneity in the material in which they propagate. Since the 1950s, both normal-mode and ray based surface wave studies have provided valuable insight into the structure of the lithosphere and mantle [Romanowicz, 2002].

Displacement from surface waves decays with depth according to frequency. Surface wave displacements can transmit stresses capable of triggering earthquakes into the crust's seismogenic zone [Ben-Menahem and Singh, 1981]. Recent studies have begun to quantify the conditions necessary for triggering, primarily in terms of stress and strain in relationship to fault geometry [Brodsky and Prejean, 2005; van der Elst et al., 2010; Hill, 2010]. Current triggering thresholds for shallow earthquakes and deep tremor have been found to be around a few kilopascals [KPa] for identified events [Brodsky and Prejean, 2005; Peng and Gomberg, 2010]. For comparison, standard atmospheric pressure is about 101 KPa. The stress drop associated with a typical large earthquake is on the order of 1-10 MPa, and tidal stresses are no more than a few KPa. Why

triggering is not more common considering the large amplitude of surface waves is an active area of research. Recently, evidence of frequency-dependent triggering has been found, but no general relationship between amplitude and triggering has been identified [Brodsky and Prejean, 2005; Guilhem et al., 2010; Chao et al., 2012].

The phenomenon of antipodal focusing (i.e. ~180^o on the other side of the Earth) has also been observationally documented and investigated [Rial and Cormier, 1980]. However, the antipodes of most recent great earthquakes occur in the deep ocean, creating difficulty in studying potential triggering associated with them. Ideally, when the surface waves of great earthquakes come back to the epicenter after traveling 360^o around the Earth, we would expect to see higher surface wave amplitudes due to similar superposition effects. For example, on December 26, 2004 a M9.0 megathrust earthquake occurred off of the coast of Sumatra, Indonesia on the interface of the India and Burma plates. The event had unusually long rupture duration of ~ 600 seconds corresponding to slip on approximately 1200 kilometers of the subduction megathrust. The average displacement was roughly 15 meters [Lay et al., 2005]. **Figure 1** shows the global displacement wave field of the M_w 9.0 Sumatra-Andaman Islands earthquake as recorded by the vertical component of the Global Seismographic Network (GSN). The R_1 to R_4 Rayleigh waves and their overtones are clearly evident with vertical ground motion of 1 cm or more. The closest station is PSI located in northern Sumatra at approximately 3 degrees near the epicenter. This station recorded clear R_n waves refocusing around the epicenter after propagating around the globe multiple times. In particular, a M7.2 aftershock occurred shortly after the predicted arrival of the R_2 wave trains to the epicentral region. Although the arrival of the R_2 wave and the M7.2 aftershock were not exactly coincident, this example raises

the question of whether aftershocks can be dynamically triggered by focusing of surface waves at the epicenter.

We also choose to examine the M9.0 Tohoku-Oki earthquake because of the high quality of the data available for the event. The Tohoku-Oki earthquake occurred on March 11, 2011 and is also considered a megathrust event nucleating where the Pacific Plate is subducting beneath the Eurasia plate near the Japan Trench although the exact dynamics in this region are still being debated. In contrast with the Sumatran event, the Tohoku-Oki earthquake had a far more compact source and consisted of multiple events but the global displacement wavefield still shows significant energy in the R_2 arrivals (**Figure 2**).

In addition to providing a better understanding of the physical mechanisms of earthquake triggering, the phenomenon of aftershock triggering by multiple surface waves of the mainshock is also of practical importance. If large earthquakes can trigger other events of significance, then perhaps there exist times after the mainshock in which the seismic hazard for a region is temporarily increased. Hence, it is important to determine whether or not delayed triggering is occurring in the epicentral region.

1.2. Previous Studies

Numerous studies of teleseismic earthquake triggering exist but focus on triggering of earthquakes by surfaces waves far from outside the aftershock zone [Peng et al., 2010; Peng et al., 2011a; Gonzalez-Huizar et al., 2012]. The ability of the Sumatra-Andaman event to trigger earthquakes at teleseismic distances due to its large amplitude surface waves (e.g., **Figure 1**) has also been well studied [e.g., West et al., 2005; Miyazawa and Mori, 2006; Peng et al., 2009; Wu et al., 2011]. Two studies of instantaneous triggering of large-magnitude earthquakes by seismic waves of the mainshock are known [Lin, 2010; Lin, 2012]. However, such instances appear rare.

In particular, Parsons and Velasco [2011] did not find any compelling evidence of instantaneously triggered $M_w > 5$ earthquakes by $M_w > 7$ events over the past thirty years. However, they did not examine the 180^o (antipodal) or the 360^o special cases, and their mainshock magnitudes may be too small to excite large amplitude surface waves at such distances. Indeed, Pollitz et al., [2012] found a transient increase of global seismicity with $M_w > 5$ immediately after the 2012/04/11 M_w 8.6 Sumatra earthquake, likely due to Love wave triggering. In summary, no detailed studies of the ability of surface waves circling around the Earth to trigger additional aftershocks have been conducted.

CHAPTER 2

DATA AND METHODOLOGY

Here, we examine the aftershocks of shallow great earthquakes (with depths ≤ 75 km) and of M_w ≥ 8 since 1990 for evidence that the returning surface waves can dynamically trigger additional aftershocks [Okal and Romanowicz, 1994]. To test this hypothesis, we search for statistically significant rate increases in aftershocks in the first few hours when the surface waves return back to the epicenter. We use earthquake catalogs reported by various network agencies and augment these with an early aftershock catalog of waveform detected events for the most recent M_w9.0 Tohoku-Oki earthquake [Lengline et al., 2012].

2.1. Catalog Sources

A catalog may be defined as a description of earthquakes giving the location, origin time, and magnitude of each event. Seismicity catalogs are by nature heterogeneous, therefore the aforementioned parameters may be composed of events obtained by various location methods, different magnitude scales, and both human and machine error contributes to the overall quality of the catalog. The instrumental catalogs used in this study contain events beginning in 1990 and are produced from digital data obtained from dense seismic networks with automatic or semi-automatic processing protocols, as opposed to historic catalogs in which events were recorded on analog instruments. The most meaningful parameter in this study is the magnitude of the earthquake for reasons that are explained in section 2.4. Since this is a statistical study, one must check and verify the data at each stage of processing to ensure as little bias as possible has been introduced into the analysis.

We use several sources of catalogs for this study. To define the mainshocks, the Advanced National Seismic System (ANSS) catalog is used. The ANSS catalog is a compilation of global

catalog data reported by various member networks. With the exception of the Tohoku-Oki event, all aftershock data also comes from the ANSS catalog as well. Most of the mainshock-aftershock sequences do not have local high quality catalogs within the first day since the events are in remote areas; furthermore, dense temporary networks are usually deployed after an event, causing difficulty in obtaining spatially dense data in the first few days unless permanent stations are situated near the epicenter. The only exception is the 2011 M_w 9.0 Tohoku-Oki, Japan event. Japan has the densest seismic network coverage of any region in the world which allows for catalogs of very high quality in terms of the number of events recorded at a given magnitude. In this study, we use both standard catalog data from the Japan Meteorological Association (JMA) and the HiNet catalog from the National Research Institute for Earth Science Disaster Prevention (NIED).

Finally we use data obtained from waveform cross-correlation analysis for the Tohoku-Oki sequence [Lengline et al., 2012]. This technique utilizes verified seismic events as a waveform template, or "matched filter", and then searches the continuous waveform data to identify similarities between waveforms. The algorithm determines the degree of similarity by calculating the mean correlation coefficient. If the coefficient reaches a specified threshold, then a new event has been found. The ‘matched filter’ procedure may yield false positives; however, the ratio of false positives to actual detections is estimated to be considerably less than one per day [Shelly et. al., 2007]. To date, the technique has yielded catalogs which contain possible observations of many more events than were previously reported [e.g., Peng and Zhao, 2009; Meng et al., 2012].

Here we use the catalog prepared from data collected from the Tohoku-Oki event [Lengline et al., 2012]. The first twelve hours utilizes a mix of waveform detections and JMA events, and

the later times use events listed only in the JMA catalog. In future studies, combining known empirical frequency-magnitude relationships with earthquake catalogs consisting of waveform detections should allow better estimation of the number of missing events at a given magnitude, at least for great earthquakes. With this data, one could attach more significance to observed changes in seismicity rates due to unexpected or anomalous activity in the early hours of earthquakes.

2.2. Aftershock Zone Selection

The spatial extent of an aftershock zone depends upon multiple factors, the foremost being the extent of the mainshock rupture. Usually aftershock activity is observed in the immediate vicinity of the fault rupture, generally corresponding to the fault surface that has experienced relative motion, or slip, during the earthquake. Typically, the magnitude scales with the observed rupture size; hence the number of aftershocks increases with the size of the earthquake. The spatial extent of aftershock activity is then expected to be greater for larger earthquakes. As a starting point, we use the relationship asserted by Kagan [2002] with

$$r = 20 * 10^{\frac{(m-6)}{2}} \text{ [km]} \quad (1)$$

where r is the aftershock zone radius and m is the moment magnitude of the mainshock. Visual inspection confirmed the aftershock activity was well within the boundaries estimated by the Kagan [2002] scaling rule with the exceptions of the 2004 M_w 9.0 Sumatra-Andaman Islands (**Figure 3**) and the 2011 M_w 9.0 Tohoku-Oki earthquakes (**Figure 4**). In the former, we modified the aftershock zone specifically for this event because of the unusually long rupture length and in the latter the aftershock zone was decreased due to the compactness of the source.

The classical Gutenberg-Richter (G-R) relation [1954] asserts:

$$log_{10}N(m) = a_t - b(m - M_c) \quad \forall\, M_c \leq m \tag{2}$$

where *N(m)* is the number of earthquakes with magnitude $\geq m$. The parameters a_t and b are the logarithm of the number of earthquakes with $m \geq M_c$ and the relation between the numbers of small and large earthquakes respectively. The value M_c is the catalog completeness threshold, which is introduced because of the inability of seismic networks to capture events at all magnitudes. This quantity will be discussed further in section 2.4. The G-R relationship has been show to hold from magnitudes of at least -1.3 to over 9 [Boettcher et al., 2009]. The parameter a_t is simply a constant of the distribution and m can be measured by different magnitude scales so it makes sense to transform this equation into one independent of catalog variation:

$$F(M) = \left(\frac{M_t}{M}\right)^{\beta} e^{\left(\frac{M_t - M}{M_u}\right)} \quad \forall\, M_t \leq M \leq \infty \tag{3}$$

$$\beta = \left(\frac{2}{3}\right) b \tag{4}$$

where M_t is the moment completeness threshold, and M_u is an empirical upper corner moment at large magnitudes. Several studies have shown that that the particular value of β in equation (4) or b value in equation (2) may reflect changes in the physics of the source, style of faulting, and/or tectonic regime [Okal and Romanowicz, 1994; Kagan, 2010].

The depth at which aftershocks are included is constrained to shallow events ≤ 75 kilometers. The majority of aftershocks used in analysis are produced at much shallower depths (**Figure 5**, Table S1). However, past calculations of earthquake parameters typically do not constrain depth [Frohlich and Davis, 1993].

2.3. Data Selection Criteria

To test the hypothesis stating a statistically significant rate increase in aftershocks occurs in the first few hours when the surface waves return back to the epicenter, three different catalog data sets were analyzed. The different data sets include aftershocks within the one day of the 2004 Sumatra-Andaman earthquake, within one day of the 2011 Tohoku-Oki earthquake, and aftershocks of $M_w \geq 8$ events (i.e. the stacked data), which are stacked to improve coherence. Time shifting of mainshocks for stacking to obtain better estimates of spatial decay parameters has been done previously [Davis and Frohlich, 1991; Nyffenegger and Frohlich, 1998; Tosi et. al, 2010]. For the stacked data, the mainshocks and their aftershocks were selected from the global ANSS catalog and range from 1990 to 2012. A mainshock was defined as an event not considered as an aftershock of any previous larger event within 100 days. All mainshock/aftershock sequences were tested for uniqueness in order not to duplicate data, and a listing for selected events is shown in Table S1. If the mainshock contained more than 20 aftershocks, the event and its aftershocks were included in the stacked data. A value of 20 represents the threshold below which determining a magnitude of completeness becomes difficult [Woessner and Wiemer, 2005] and was chosen for this reason. The majority of events had an order of magnitude more aftershocks than the selected threshold. We use the ANSS catalog for the Sumatra-Andaman sequence, and a catalog containing a mixture of JMA and waveform detected events for the Tohoku-Oki event. To avoid biasing the event stack, we use aftershocks listed in the ANSS catalog for the Tohoku-Oki event stack data. The aftershocks for a given mainshock were chosen using a temporal constraint of one day, and the spatial extent of the aftershocks was defined using an aftershock zone scaling relationship [Kagan, 2002] as discussed in Section 2.2.

2.4. Magnitude of Completeness

Determining which aftershocks should be used to calculate both rate and aftershock decay parameters (e.g., Omori's law) is of critical importance. The current criterion used is the magnitude of completeness, M_c. The magnitude of completeness is the smallest value of magnitude at which the catalog is thought to have included all seismic events. Missing events in the catalog most commonly occurs because the events are (1) too small to be detected at enough stations and, therefore, cannot be located, (2) stations may not be physically capable of recording events of a very small size and/or the amplitude of such events may be below the noise level of a station, and (3) aftershocks may be hidden in the coda of larger events. The coda is defined as that portion of the direct phase wave train which is scattered and arrives following the main phase over an extended time interval [Sato and Fehler, 2012].

As Woessner and Wiemer [2005] point out, this definition is somewhat dependent on the functional form of the assumed frequency-magnitude distribution. A correct estimate is important because overestimating leads to usable data being discarded while underestimating leads to incorrect estimation of other parameters which depend upon the M_c, such as the G-R *b* and Omori *p*-values [e.g., Utsu et al., 1995]. For example, if the M_c is underestimated, then the *b*-value will be incorrect because there will be less cumulative events above the M_c cutoff than expected and the behavior will not be strict power-law. Consequently, underestimation of the M_c value will cause the *b*-value to be lower than the actual value. Another potential issue is overestimation due to magnitude indeterminacy. Difficulty in magnitude determination tends to occur for small events, and any systematic error will skew the estimated *b*-value. In this study, the M_c is usually large, so missing events are of greater concern than incorrectly determined magnitudes.

Two distinct methodologies of estimating the M_c have been demonstrated in the literature. One class of methods uses data from the seismic network either from phase-picks or waveform data [Woessner et. al., 2010]. In principle, such methods are potentially more accurate as well as more time consuming and have not been thoroughly investigated in the context of this study. The other class is a catalog based, statistical approach [Wiemer and Wyss, 2000; Woessner and Wiemer, 2005]. These methods rely upon the accurate interpretation and usage of waveform and phase-pick data, and, therefore, are perhaps more prone to error. However, for the relativity high M_c values found here, catalog methods are likely unaffected by such issues since the magnitude and location of larger earthquakes are more accurately determined. Human errors can contribute to a systematic catalog bias, but, because the events are stacked the absence of a few events, would have minimum impact on the overall result.

More importantly, the magnitude of completeness M_c may change unpredictably with time for different sequences. Obtaining a precise M_c value during an aftershock sequence is a difficult problem. A quick check used compares the M_c at short times, such as a day, with that of longer times (e.g., months) to ensure that large variations do not bias the estimation at the short times. The M_c would be expected to decrease in time as well [Kagan, 2004]. For this study, the time periods of interest are 1 day and 100 days. The M_c for either time period does not fluctuate significantly (Table S2).

The M_c for the aftershock sequences was determined by using both the entire magnitude range (EMR) method with bootstraps and the corrected maximum curvature method (MAXC) [Woessner and Wiemer, 2005]. In particular, because of small sample sizes and a short time window, the EMR method generally produced better values than the MAXC method with regards to identifying a reasonable M_c value. The MAXC method can become trapped in local

minima when trying to determine the magnitude of completeness. Adding a correction factor of 0.2 to the MAXC results generally agreed with the magnitude of completeness calculated from the EMR method [Woessner and Wiemer, 2005]. Another way to check the obtained M_c against the frequency magnitude distribution is to estimate the *b*-value for a M_c range around the value found by EMR and MAXC to test its sensitivity to the catalog cutoff. A straightforward estimate of *b* is given by:

$$b_{est} = \frac{\log_{10} e}{\overline{M} - (M_c - 0.05)} \tag{5}$$

where $\overline{M}$ is the mean magnitude and the 0.05 is a correction factor associated with the typical 0.1 magnitude binning. Marzocchi and Sandri [2003] demonstrate that this formula yields reliable estimates even in the presence of measurement error in a small catalog.

The variation of the maximum likelihood estimate of the *b*-value with the M_c value was also calculated. As Table S2 shows, the M_c varied between 4.6 and 5.2 for the individual sequences. However, in some instances, too few aftershocks were available to calculate a magnitude of completeness for a mainshock event using a particular method. The aftershock sequences with a reasonable M_c value were then added to a stack to improve coherence as indicated in Table S2. A total of fifteen mainshocks aftershock sequences are used in the final stack, resulting in approximately 2763 aftershocks in a twenty-four hour period.

2.5. Stacking and Rate Method

Due to potential variation and incomplete catalogs for each sequence, we stack all possible sequences in order to improve the coherence of any signal that may be partially expressed in the individual sequences. If surface wave triggering exists, at worst, stacking would tend to smooth out a signal, as the operations are additive. At best, stacking would sharpen a peak in either

moment or number rate when the surface waves return to the mainshock epicenter. Because of the small number of sequences and the number of total samples, stacking incoherent signals is a potential issue. For this reason, both the rate and moment rate are calculated and compared to the timing of the incident surface waves. By doing so, the chances of a purely random fluctuation are lessened, though not completely ruled out.

Multiple approaches have been developed to calculate statistically significant seismicity and moment rate changes. Two currently used approaches are the standard deviate, *z* [Habermann, 1988] and the β [Matthews and Reasenberg, 1988] value. The β value is given by the equation

$$\beta_n(n,\delta) = \frac{M(t,\delta) - n\delta}{\sqrt{n\delta(1-\delta)}} \tag{6}$$

where *n* is the number of earthquakes for both time periods, *t* is the normalized end time of the interval of interest, δ is the normalized length of the interval and *M(t*, δ) is the number of the events in the interval defined by end time *t* and duration δ. Essentially, this method computes the difference between the observed and expected number and normalizes by the standard deviation. However, the β value is sensitive to the size of the data set used, relying upon the fact that a Poisson distribution tends to a Gaussian distribution for calculating probabilities. However, the use of the β value in this study is precluded because the β value assumes that earthquakes are independent of one another, so the catalog must be declustered which means aftershocks are removed. The β method also assumes a uniform rate of background activity which is not applicable during an active aftershock sequence. In contrast, the standard deviate is a symmetric extension of the β statistic:

$$z = \frac{R_1 - R_2}{\sqrt{\left(\frac{\sigma_1^2}{n_1} + \frac{\sigma_2^2}{n_2}\right)}} \tag{7}$$

where R_i is the number of earthquakes in the ith period, n_i is the number of bins of length T_{bin} into which the ith period is subdivided and σ_i is the standard deviation of the number of earthquakes in T_{bin}. Values of z which use different sample sizes or window lengths cannot be directly compared. As before, z values are meant to be used on declustered data, so neither method can be applied to this study. The background activity composed of independent mainshocks is assumed to occur as a stationary Poisson process. However, the previously mentioned methods are used to find trends that are non-stationary with regards to the background activity. During an aftershock sequence, the aftershocks are a result of a non-stationary process and so rate changes cannot be identified by these measures.

Because of the lack of a stationary background, absolute changes in rate will be difficult to identify, so instead this study focuses on identifying relative rate changes using a moving window approach for both seismicity and moment rates. The rates were calculated using a fixed event window and were also tabulated using a moving average approach with varying time windows for comparison. Both central and forward moving averages in time were calculated for various time window sizes. Fixed event-size windows were also used to calculate rate changes. We present the moving average results to directly compare different stacks because the size of the time window is fixed. In order to quantify a rate increase, we use a forward moving average. Central moving averages also may be used but the method is not symmetric near zero times leading to artifacts. The time window chosen has to balance temporal resolution with sensitivity to artifacts. We find time windows corresponding to values between 15-45 minutes do not strongly affect the result (**Figure 20**). The fixed event size windows yielded similar results, but

cannot be directly compared. Fixed event windows also may be more prone to errors with data more sparsely distributed in time.

2.6. Modified Omori Law Fits

The decay of aftershock activity following a mainshock follows a power law known as the Omori law [Omori, 1894]. In its current form, the power law is referred to as the Omori-Utsu or modified Omori law (MOL) [Utsu, 1961]. Changes in the temporal rate can be detected by employing various transformations of the Omori-Utsu model [Ogata, 1988; Utsu et al., 1995].

The MOL takes the form:

$$\lambda(t) = n(t) = \frac{K}{(t+c)^p} \tag{8}$$

where *n(t)* represents the frequency of aftershocks per unit time interval, *K* measures the productivity of the sequence, *c* adjusts for missing earthquakes in the catalog and *p* determines how quickly the activity falls off to the constant background intensity which as before, was presumed also to be a stationary Poisson process. A point process is called a stationary Poisson process if the following conditions hold:

I. Independent Intervals. The number of events occurring in two disjoint time intervals is independent of each other.

II. Stationary. The probability distribution of the number of events falling in a time interval only depends on the length of the time interval.

III. Simplicity. Two are more events never occur simultaneously.

The value of *p* typically ranges between 0.6 and 2.5 with a median of 1.1 [Utsu et al., 1995]. Higher *p* values tend to characterize earthquake swarms as may be observed in geothermal or volcanic regions [Ben-Zion and Lyakhovsky, 2006]. Smaller *p* value have been associated with superimposed aftershock sequences, since the decay would occur more slowly than expected due

to multiple events with some time separating them contributing aftershocks to the sequence. No dependence of *p* with mainshock magnitude has been found [Nyffenegger and Frohlich, 1998]. The value *c* is often presumed positive and is thought to be an artificial constraint introduced by the incompleteness of catalogs at early times [Kagan, 2004]. Ideally, if all earthquakes were captured, the *c*-value would tend towards zero. However, Kagan [2004] argues that *c* is actually negative, otherwise, the singularity in the equation occurs before the mainshock.

In either case, when using real catalogs at short times and performing an MOL analysis, the estimation should be checked by examining changes in the M_c with time. Such arguments reinforce the fact that the parameters *p*, *c*, and *K* introduced by the MOL can obscure the physical underpinnings of seismicity, so recent research has focused on finding laws in terms of quantities such as moment [Kagan and Houston, 2005], rather than number of earthquakes. Utsu et al. [1995] commented that if aftershock sequences do obey a MOL with *c* equal to zero, that "... such a large percentage of missing events seems unlikely for many of the aftershock sequences to which relatively large c values have been estimated." However, in light of recent evidence of significant numbers of waveform detections, the mentioned scenario may actually be true [e.g., Peng et. al., 2006, 2007; Enescu et al., 2007]. Therefore, defining completeness in terms of moment or another physically measurable quantity may be a more sensible approach. The uncertainty suggests the MOL should be considered as the time-dependent intensity function $\lambda(t)$ of a non-stationary Poisson process which models aftershock activity and physical interpretations of its parameters must be carefully scrutinized. The MOL represents a Poisson process which has a time variable rate violating assumption II, but this variable rate is independent of the occurrence of other events implying assumption I still holds. The MOL can be integrated between times [S, T] analytically to obtain:

$$\tau = N(S,T,p,c,K) = \begin{cases} \dfrac{K[(T+c)^{1-p} - (S+c)^{1-p}]}{(1-p)} & p \neq 1 \\ \mathrm{K}[\ln(T+c) - \ln(S+c)] & p = 1 \end{cases} \quad (9)$$

where *N* represents the total number of events between times [S,T]. *N* is also referred to as τ which is the frequency-linearized or transformed time [Ogata, 1988]. If one has chosen the proper parameters for the Omori law, then the integration transforms the integrand into a stationary Poisson process with constant intensity. This may be dependent upon the choice of the lower time bound, *S*, after which the MOL holds. A transform time analysis yields the cumulative number of events for a particular fit and allows for comparison based upon the examination of the predicted cumulative values compared to the observed values. Past studies have used the transform time to estimate when an aftershock sequence is perturbed from or returns to its background rate [Ogata, 1984]. One then compares the cumulative number of aftershocks to the transformed time, which should both plot along a straight line as long as the occurrence of aftershocks is above the background rate. Typically these studies attempt to estimate changes many days from the mainshock occurrence by fitting the Omori-Utsu model early in the aftershock sequence and predicting days or weeks ahead. In contrast we applied the same technique within the first day of the mainshock event.

In practice, obtaining accurate estimates of the MOL parameters is a non-trivial endeavor. The most common way is using the log-likelihood function (LL) of the MOL. The times of the events $\geq M_c$ are the input data. The LL is then maximized with respect to *p*, *c*, and *K* which yields estimates and their associated errors. When combined with the G-R law, it becomes possible to forecast the probability of large aftershocks based upon observed data in the region or similar ones [Reasenberg and Jones, 1989]. A severe shortcoming of the MOL is the complete non-consideration of the existence of secondary, tertiary etc clustering of aftershocks. Clustering

and dependence of events violates assumption II above. The self-excitation of aftershocks effectively changes the intensity rate to be a function of its previous history. As a result, the fit to the MOL may be poorer than expected, which is further exacerbated at short times because the aftershock activity is more vigorous and can fluctuate markedly.

2.6.1. MOL Analysis of Data

Only data at and above the M_c was used in the MOL analysis. The MATLAB code used to calculate the magnitude of completeness was obtained from Dr. Jochen Woessner [personal communication, 11/21/2011] based upon their previous paper [Woessner and Wiemer, 2005]. For this study, we also used a modified version of the ZMAP [Wiemer, 2001] MATLAB code to solve for the MOL parameters at 1 and 100 days for the stack and the Tohoku-Oki event according to equation (8). With reference to the stack, the MOL calculation requires a mainshock, and so a composite mainshock of the mean of the stack, 8.32, was used. Our approach is acceptable, because the *p*-value does not depend upon the mainshock magnitude. In contrast, the *p*-value will depend upon the length of the training period which is defined as the interval of time during which the aftershocks will be fit to the MOL. Unfortunately, no agreed upon procedure for choosing *p* exists in the literature. General guidelines include the time period (1) should start when the catalog completeness may be changing but becomes calculable (2) must include the largest aftershock in the sequence in that interval and, (3) should be long enough such that extrapolation is meaningful. For both stacks, the MOL was fit to the entire time period in order to estimate the parameter *c*. We then compared *c* visually with the observed clustering and cumulative aftershock plots. The estimated *c* was then used as the cut-off for the lower time period and the MOL parameters were recalculated. The upper times used were 1 and 100 days

and were chosen because backward extrapolation is desired as opposed to forward extrapolation, so all of the available data at the M_c should be used for parameter estimation.

Once the parameters *p, c,* and *K* were obtained, the transform time equation (9) was plotted against the observed seismicity. Using the estimate of the 100-day parameters, the rate was backwards extrapolated to 1 day and compared against the observed seismicity in order to detect seismicity rate changes.

2.7. Synthetic Models

All stochastic models of seismicity are incorrect to some degree. In order to make more accurate statistical inferences, baselines for comparisons must be found. Synthetic catalogs that hypothetically describe seismicity are desirable. Synthetic modeling methods derived from them will reflect those shortcomings. However, some models have features that are useful to test particular hypotheses against. It is possible to generate synthetic aftershock timings from the MOL. However, the MOL may not accurately reflect the true characteristics of the aftershock sequence, especially at early times after the mainshock. If the fit to the MOL is poor, then timings generated by such methods will only be as good as the original parameter fit. At worst, the fit may reflect a simple exponential power law decay. The MOL can be used, and typically smaller independent mainshocks will conform to assumptions I and II. However, larger mainshocks will generate aftershocks that will excite further aftershocks. Although aftershock seismicity is a spatiotemporal occurrence, I neglect the spatial modeling of the aftershocks because we are not addressing variability in space and time in this study.

Currently, the Epidemic Type Aftershock Model (ETAS) is the most widely used synthetic model [Ogata, 1988]. At its core, the ETAS model assumes that every aftershock can trigger further aftershocks according to externally imposed constraints and the occurrence rate can be

described by a superposition of MOL functions shifted in time. The intensity function at time *t* given the history H_t for the ETAS model is given by:

$$\lambda(t|H_t) = \mu + K_0 \sum_{t_i<t} \frac{e^{\alpha(M_i - M_0)}}{(t - t_i + c)^p} \tag{10}$$

In this model, μ is a constant occurrence rate for background seismicity, the sum is taken for all earthquakes *i* occurring before time *t*. The productivity of each earthquake of magnitude M_i is determined by the parameter K_0 and by the exponential term containing α. In other words, the value of the productivity affects the total number of synthetic daughter events created in all generations. Alpha, α, is a parameter which assists in determining how many earthquakes a particular event triggers. Both K_0 and α must be estimated using the observed data. The ETAS model is branching meaning that a daughter earthquake has only one unique mother earthquake. However, each unique mother earthquake may have a one-to-many relationship with its daughters. Physically, there is no reason why triggered earthquakes could not share several parents. However, this is a "mean-field" constraint imposed to simplify the process while qualitatively retaining the physics. The cut-off value M_o is equal to the M_c of the data that is being modeled in this study. This cut-off is necessary to ensure that too many events are not generated for larger mainshocks. The most important parameter is not explicit in the functional form of the ETAS intensity. This key parameter is known as the branching number, *n*. The branching ratio is the average number of daughters created per mother event [Helmstetter and Sornette, 2002]:

$$n \equiv n_0 \int_0^{\infty} \frac{dt}{(t+1)^{1+\theta}}, \tag{11}$$

$$\text{where} \quad n_0 \equiv \frac{K_0}{c^{\theta}} \frac{b}{b-\alpha} \quad \text{and} \quad \theta \equiv 1 - p \tag{12}$$

The parameters are the same as in the ETAS equation; however, the G-R equation determines the *b*-value. The value of the branching number determines various regimes in which the seismicity diverges or converges. Hence in practice, using the ETAS equation is not always straight forward. The ETAS model requires initial parameters obtained from MOL fits; however, these estimates are somewhat sensitive to the conditioning of the data through the choice of the magnitude of completeness and the time interval assumed for the fit.

We attempted to use two codes to generate suitable synthetics. Both programs model aftershock activity by assuming an ETAS process. The first code AftSimulator.m runs in MATLAB and is provided by Dr. Karen Felzer publicly on her website [Felzer, 2012]. The code simulates both the spatial and temporal decay of aftershocks [Felzer et al., 2002; Felzer and Brodsky, 2006]. The code is based upon work by Ogata [1988]. The second software package is SASeis2006 [Ogata, 2006]. SASeis2006 is a collection of routines written in FORTRAN which enable the user to solve for the MOL parameters and model synthetic aftershocks based upon those parameters.

The input parameters of SASeis2006 must be determined from an existing set of mainshock-aftershock sequences, making it difficult to generalize synthetic generation using this code to regions with little data because the input parameters will be poorly constrained. In particular, μ and K_0 are difficult to determine consistently because they must be calculated and observed over long periods. However, once values have been set, SASeis2006 generates synthetic times using a pseudorandom number generator and employs an acceptance-rejection method known as

thinning. In order to "thin", one finds a constant rate function λ_0 which serves as an upper bound for equation (10). One then generates synthetic times using the constant rate and compares the ratio of $\frac{\lambda(t|H_t)}{\lambda_0}$ to a random number on (0,1). If the random number is less than the ratio, then we keep the time. If not, we discard it and try again. Mathematical arguments can show that this process will approximate a simple nonhomogenous Poisson process. SASeis2006 generates the initial seed magnitudes by using the inverse G-R formula:

$$Mag_{synthetic} = -\frac{\log_{10} U(0,1)}{b} + \ cutoff\ magnitude \tag{13}$$

where $U(0,1)$ is a uniform random number on (0,1) and the cutoff magnitude is a user supplied magnitude threshold for all generated magnitudes. However, the code only generates aftershocks for one generation, meaning that it does not track the parent aftershocks of the produced children or vice-versa.

The code of Dr. Karen Felzer uses a different approach and solves for the inverse of the nonhomogenous Poisson process directly. The MATLAB program uses a starting productivity value A_D that has to be found for each sequence to be simulated [e.g., Felzer et al., 2002] and this value is not the same as the K_0 in equation (10). The code generates aftershocks and branches according to a stopping criterion. If the criterion is not reached, new aftershocks are generated by using each "active" parent aftershock. The code does not allow for multiple parent earthquakes to trigger one or more daughter events. Only multiple children of one parent are allowed. Although this approach is better grounded in physics than SASeis2006, it requires determination of the productivity of a sequence by rather ad-hoc determination. For example in Felzer et al. [2002], the MOL parameters were found using forward modeling by minimizing the least squares residual between the model and observations for the number of aftershocks above

magnitude two in the first five days. Why these specific numbers were chosen is not explained. Another issue is the inability to relate Felzer's productivity value to Ogata's productivity constant [Felzer, personal communication, 2012]. My investigations have concluded that regardless of which software package is used, some synthetic sequences may have non-unique MOL parameterizations. At long time periods this may not matter, since the MOL exhibits a smooth decay and gradual accumulation of events. However, for short time periods mimicking the dynamics is important since the power law expression of these dynamics will affect the observed number rate fluctuations. The erstwhile issues somewhat negate the value of these synthetics with respect to backwards extrapolation of the MOL since the number rate may differ erratically.

2.8. Summary of Analysis Procedure

To summarize, the analysis procedure consists of the following steps: (1) the aftershock zones for the stack data consisting of fifteen mainshocks and two separate events were determined; (2) the aftershocks were then stacked into a one-day and 100-day sequences; (3) after stacking, the inter-event times were calculated and compared to the randomized times for the stacked sequence in order to examine the inter-event time frequency distributions for trending in the stacked data; (4) histograms of depth and magnitude distribution were created; (5) the data were cut at the magnitude of completeness M_c, and then MOL and G-R parameters were found; (6) both seismicity and moment rates were calculated for all sequences; (7) data up to 100 days were also fit to the MOL parameters and then backwards extrapolated to examine trends away from expected behavior for the stacked data and two events; and (8) synthetic sequences were generated using MOL parameters and compared to the observed sequences.

CHAPTER 3

RESULTS

Identifying a rate increase during an aftershock sequence is challenging because although the background activity is decaying in time, the instantaneous rates may fluctuate. As briefly mentioned before, existing methods for identifying rate increases such as z or β values require removing aftershocks by declustering to identify independent events in order to establish a background rate for comparison [van Stiphout et al., 2011]. These techniques are not suitable for application to this study for several reasons: the triggered aftershocks may be removed during declustering, the triggering time interval corresponding to the surface wave arrival is small compared to the aftershock sequence duration, and stacking the results amplifies differences in the tectonic regimes to an extent where dependent events may not be separable.

The one day stacked data included 15 mainshocks with a mean magnitude of 8.3. Both the EMR and MAXC methods calculated of a magnitude of completeness of 5.0. Out of 2763 aftershocks, 981 have magnitudes greater than or equal to 5.0. The M_c value is reasonable considering that the 100-day stack yielded similar values, and a visual inspection of the frequency-magnitude plot (**Figure 6**) and binned histogram agreed with the obtained M_c. The change in the *b*-value with the M_c was also estimated in **Figure 7**. A comb plot is a useful measure of the qualitative clustering of the data and is plotted in **Figure 8a** and **Figure 8b**. The MOL parameters were determined using the M_c estimated 981 events. The cumulative, log and transform time plots for the MOL parameters are shown in **Figure 9**. Allowing for error, the MOL parameters were also estimated for the $M_c \pm 0.1$, but were not found to be particularly sensitive to this choice as shown in Table S3. We follow Kagan and Houston [2005] and plot the number and moment rate in **Figure 10**. The R_2 arrival shows some evidence of rate increase,

while the R_4 arrival is less clear. While there is no obvious increase in aftershock occurrence rate at the epicenters, there is some evidence of increase in moment rates during those times. The one-day data was plotted against the MOL parameters estimated at 100 days in **Figure 19**. The 100-day MOL parameters used in the extrapolation were estimated at the one-day M_c (5.0) for consistency (**Figure 13**), even though the 100-day stack has an overall lower magnitude of completeness (~4.7).

The 100-day stacked data was composed of the aftershocks of the same mainshocks as the one-day data and had the same mean magnitude. The M_c was found to be 4.7 using 11488 events of which 5135 were at or above the M_c. The frequency magnitude plot is shown in **Figure 11**. Comb plots are shown in **Figure 8c** and **Figure 8d**. The MOL parameters were estimated using 5135 events. The cumulative, log and transform time plots for the MOL parameters are shown in **Figure 12**. Allowing for error, the MOL parameters were also estimated for the $M_c \pm 0.1$, but were not found to be particularly sensitive to this choice as shown in Table S3. The stack data of up to 100 days was also fit to the MOL. The resulting *p*-value was close to unity, which is typical for an aftershock sequence. The MOL plots also indicate possible deviation from the expected rate behavior at early times (Figure **19**). Rate comparisons need a reference baseline, so synthetic distributions were created under uniform and epidemic type aftershock sequence (ETAS) assumptions [Ogata, 1988]. The ETAS parameters assumed were taken from performing a modified Omori law fit to the data and using the obtained parameters as inputs [Utsu et al., 1995]. The same rate calculations were then performed on those distributions and compared to the stack.

The 2004 Sumatra event (**Figure 14**) also shows evidence of modulation by the returning surface waves. The ANSS catalog data was used for this event. However, the aftershock zone

was extended by visual inspection to account for the long rupture length. The catalog data for the Sumatra event yields 298 aftershocks with 141 at and above the magnitude of completeness of 5.0. Therefore, the rates and moment do not fall off as sharply in the course of one day, and noticeably more scatter exists in the results. The MOL parameters for the Sumatra event are shown in Table S3.

A wealth of data is available for the Tohoku-Oki event due to the high quality of the Japanese seismic network. In particular, we have analyzed this event using the first six hours of a catalog consisting of events from the JMA and HiNet catalogs as well as newly detected events found by the waveform cross correlation technique of Peng and Zhao [2009] adding ~1000 more aftershocks to the analysis [Lengline et al., 2012]. The second half of the day includes events only found in the JMA catalog; however, for this study, the first 2-6 hours are most relevant.

The frequency-magnitude plot and histogram are shown in **Figure 15**. With the additional events, the catalog for the first day contains 2,305 events, and there are 682 events at and above the M_c value of 4.6. The MOL parameters are shown in Table S3 and plotted for the event in **Figure 16**. Using an 1800-s time window, evidence exists of possible modulation of aftershocks by surface wave arrivals in the first six hours (**Figure 17**). We estimated parameters for the MOL of the Tohoku-Oki data at 100 days at a M_c of 4.6 and then extrapolated to one day in **Figure 18**.

Using both the codes of Ogata [2006] and Felzer et al. [2002], we found it difficult to create and stack synthetics which accurately reflected observed data in a meaningful way. For my purposes, we neglect background seismicity based upon the assumption that the background seismicity level is small compared with ongoing seismicity in the first few hours. One possible reason is the cumulative effect of repeated deviations from the G-R distribution due to stacking

of large events. The ETAS model also generates synthetic magnitudes based upon assumptions about the power law behavior of frequency and magnitude. Recently it has been suggested that deviations occur for large magnitude mainshocks (e.g., $M_w \geq 8$) and this could impact the accuracy of existing ETAS models [Wang et al., 2010]. Ultimately, the ETAS model relies upon self-excitation subject to constraint, and therefore seeks to emulate the behavior of real sequences which may be difficult if the aforementioned assumptions do not hold.

CHAPTER 4

DISCUSSION

4.1. Event Stack

Based upon the analysis of timings, my results suggest a moderate increase of early aftershock activity when the surface waves return to the epicentral region, a time period of a few hours. The increase is observed in **Figure 10** and **Figure 17**. We note that the event rate increase at later times after the R_2 arrivals is less clear, but the moment rate does shown some increase and possible correlation during the R_2 and R_4 arrivals. However, we cannot completely rule out the possibility that such an increase is purely due to random fluctuations of aftershocks or caused by missing aftershocks in the first few hours after the main shock. In addition, the magnitude of completeness may fluctuate in time. However, at almost 2.5 hours after the mainshock and for the high completeness values found during this study ($M_c \sim 5.0$), we believe the fluctuations in M_c are not an important source of error.

Ideally stacking should enhance the signal. However, we find that stacking causes difficulty in analyzing the stack in terms of the MOL [Nyffenegger and Frohlich, 1998]. Stacking may create an excess of events at short times, which complicates extrapolation from parameters estimated using larger time intervals. Although we were able to use an enhanced catalog for the Tohoku-Oki event, no such catalogs are available for other events in the stack. Different events contributed different numbers of aftershocks to the complete stack, but no attempt to normalize the individual contribution to the entire stack was made, so events may not be coherently interfering or subsets of events may contribute disproportionately. For example, the contribution of some aftershock sequences may mask or enhance a relative rate change between time intervals. However, even if our current results are caused by fluctuations, events below the

magnitude of completeness may exist which are triggered. Recent studies indicate that a large number of aftershocks may be missed in the first hours of great earthquakes [e.g., Peng et al., 2006, 2007], and our proposed effect may exist but not be discernible due to the high level of coda noise from the mainshock and large aftershocks. Furthermore, if dynamic triggering mostly occurs for smaller magnitude earthquakes [Parsons and Velasco, 2011], the possible rate increase may involve the triggering of a cascade of events all below the magnitude of completeness or perhaps a mixture of both [Helmstetter and Sornette, 2003].

We admit that these events may occur regardless of the returning surface wave effects. However, antipodal focusing may serve to advance the timings of such events. The predicted antipodal convergence does not occur at a single point, instead focusing or constructive interference occurs in a wide region around the epicenter. However, our study effectively collapses the region one dimensionally in time with no consideration of the spatial distribution of aftershocks. Surface wave triggering may occur in particular spatial domains in the epicentral region. Possible differences in aftershock behavior based upon nearest neighbor relationships in time and space may exist but the proposed techniques are not yet suitable for attempting to partition the spatial clustering of aftershocks in the early hours after a large earthquake [Zaliapin et al., 2008]. In short, triggering may occur in a particular domain in the epicentral region, and the signal may be masked by the inclusion of data across the entire aftershock zone. Alternatively, transient increases may be explained by the clustering in time and space of a particular event unrelated to surface wave triggering. The current study cannot discriminate either possibility.

The parameters of the MOL were estimated using 100 days of stacked data, but when backwards extrapolated in the first day, the predicted values were found to be generally higher

than the observed values (**Figure 19**). The stacking procedure could produce this observation, as the productivity at the M_c would be higher than expected by stacking. Essentially, the MOL will over-predict the number rate at early times for a stacked sequence, so extrapolating the MOL is difficult because of the lack of a normalization procedure for stacked aftershock data. One could choose to normalize by using a fraction of the number of the total as a weight, but then the choice seems arbitrary since many of the earthquakes are of different source dimensions and none of this is captured in such a scheme. Normalizing by moment may be more useful, but this would potentially exaggerate differences in the reporting capabilities of networks that recorded the event.

4.2. The Sumatra Andaman Sequence

The Sumatra-Andaman results indicate some modulation (**Figure 14**). However, the local network coverage was poor during the event, and subsequently, the M_c (5.0) is high on the first day. If the Tohoku-Oki event is typical, then one would expect that thousands of aftershocks are missing from the catalog for the Sumatra-Andaman sequence. In addition, the rupture length of the event was extended. Hence, a larger region must be analyzed for triggering. But this presents a problem, since it delocalizes the focusing effect over a wider area and makes it more difficult to distinguish from the expected aftershock activity.

4.3. The Tohoku-Oki Sequence

The Tohoku-Oki results share the same sources of error as the stacked sequence. However, because no stacking of the sequences was involved, inclusion of stacking related errors is unlikely. The MOL parameters were estimated for 100 days of data and extrapolated backwards (**Figure 18**). The values for the Tohoku-Oki event appear reasonable. However, a discrepancy between the predicted results and the observed rates is again observed. The Tohoku-Oki event

produced large aftershocks, which may indicate a deviation away from the Omori law at short times. In particular, intense aftershock activity may increase the expected productivity at short times and so parameter values obtained at later times may underestimate the initial intensity of aftershocks.

4.4. Triggering Mechanisms

A better understanding of the statistics of aftershocks helps inform our understanding of the physical mechanisms of earthquakes. For example, magnitude-frequency relationships are observable manifestations of earthquake producing systems. One can attempt to separate the rupture process from the triggering criteria that induces it. Stress drop associated with slip has also been asserted as a proxy for aftershock productivity [Helmstetter et. al., 2005]. The underlying physical reason may be associated with differences in mechanical strength on the fault (e.g. asperities) and may change with time as the aftershock sequence evolves, but mapping such a situation is difficult at short times.

Coulomb stress changes may be calculated using an earthquakes slip distribution and then the aftershock distribution are compared to the calculated field [King et al., 1994]. Specifically, stress shadows may influence the spatial extent of aftershock occurrence; however, such processes are typically modeled on the order of days after the mainshock [Felzer and Brodsky, 2005]. Shadows are associated with static or quasi-static processes caused by the mainshock slip and are not considered relevant to the universal rate increases associated with dynamic triggering in the early hours after mainshock.

Dynamic triggering may occur in part to rate and state frictional dependence [Dieterich, 1994; Parsons, 2005]. Whether an aftershock is triggered or not may depend on the orientation of the potential aftershock region with respect to the mainshock, and the magnitude of the

loading. Surface wave displacements may change the loading rapidly in a frictionally locked region which depending upon geometry, may promote or inhibit frictional failure. If a region does not fail concurrently with surface wave passage, the region may be still susceptible to stress corrosion or other secondary processes induced by the surface wave. Stress corrosion occurs when a change in loading accelerates crack growth which shortens the time to failure. Fluids are known to reduce stresses on faults, and the movements of fluids in the subsurface due to perturbations by the mainshock and aftershocks may promote failure [Kanamori and Brodsky, 2004]. However, research is still quantifying the timescales on which such processes act. Finally, a combination of all of these processes may occur to explain the aftershock seismicity patterns observed. If studies such as ours can positively identify transient changes in aftershock rates, then we may be able to better understand a great earthquake in the context of a system of interacting events, rather than an isolated one.

CHAPTER 5

CONCLUSIONS

Identifying a rate increase during an aftershock sequence triggered by returning surface waves has not been attempted previously. The results presented in this study admit the possibility of the phenomenon. Existing methods for identifying rate increases focus on removing aftershocks by declustering to establish a background rate. Rates must be calculated from a sequence of aftershocks with an accurately estimated magnitude of completeness. Overestimating the M_c may mask structure in the data; however, underestimating may lead to incorrect conclusions. Complications arise because it is possible that the earthquakes being triggered fall below this completeness threshold. Alternatively, even if triggering does occur above the completeness magnitude, it would have to generate enough activity to indicate statistically observable deviations from the assumed distribution. Transform time analyses based upon the MOL may not see small, transient rate increases since such methods examine cumulative departures from expected behavior.

We have found that (1) the Sumatra data is inconclusive owing to its sparse nature, (2) the event stack shows possible evidence of rate change, (3) the Tohoku-Oki event also shows possible evidence of rate modulation. The results cannot be regarded as conclusive, since in the absence of adequate synthetic sequences for comparison, the statistical significance is difficult to assess. The large number of detections found at high magnitudes during the Tohoku-Oki sequence may indicate a break in the classical G-R behavior, which has been theorized by previous studies [Kagan and Houston, 2005]. Accurate synthetics should be able to reproduce this behavior. But existing software does not generate the current clustering seen in the Tohoku-Oki results without a-priori and somewhat ad hoc assumptions. In addition, newer Bayesian

methods of MOL parameters estimation may prove more accurate, because the use of priors can possibly build-in the self-similar nature of earthquake occurrence [Holschneider et al., 2012]. But whether a change in formalism will inform our understanding of the aftershock process remains to be seen.

Future work may need to focus on a spatial and temporal investigation of triggering using the Tohoku-Oki catalog [Lengline et al., 2012]. Resolving the correlation between surface waves and aftershock triggering may be easier if a particular spatial domain is selected. In particular, since waveform data for the Tohoku-Oki event is available, the move out of the Rayleigh and Love waves with respect to stations in Japan should be more evident [e. g., Miyazawa, 2011]. Recent topological studies of aftershocks suggest more natural classifications that are statistically distinct [Zaliapin et. al., 2008]. Aftershocks tend to cluster, and if one could resolve the particular clustering, it would be interesting to compare clusters of aftershocks to surface wave activity since the clusters may show better correlation. Currently, the seismological community has no general consensus of the most appropriate synthetic model to use. Ultimately, assertions pertaining to seismic hazard must be supported by unambiguous evidence; otherwise their validity is called into question. Unfortunately, lack of consensus makes comparing the results of publications using different simulation techniques difficult. Furthermore, comparisons of observed data to different synthetic models may yield different statistical significance that complicates evaluation of the associated hazard. We believe these problems demonstrate the need for synthetics that can accurately represent aftershock activity.

FIGURES

Table S1. Event list

Event Name	M_w	Date	# Events Found 1 day / Mc*	# Events Found 100 day	Mc	Radius (km)	Depth (km)
Guam	8	1993/08/08 08:34:24.93	27	125	4.7	200	59
Japan-NE	8.1	1994/10/04 13:22:55.84	158	556	4.8	224.4	48
West-Papua	8.2	1996/02/17 05:59:30.55	197	436	4.6	251.8	33
NewIreland-Papua	8	2000/11/16 04:54:56.74	116	590	4.8	200	33
Peru-Southern	8.4	2001/06/23 20:33:14.13	126	238	5.0	317	33
Hokkaido	8.3	2003/09/25 19:50:06.36	31	213	4.9	282.5	27
Sumatra-Andaman	9	2004/12/26 00:58:53.45	298	1287	4.8	632.5	30
Tonga	8	2006/05/03 15:26:40.29	51	222	4.9	200	55
Kuril Islands	8.3	2006/11/15 11:14:13.57	304	942	4.8	282.5	10
Solomon Islands	8.1	2007/04/01 20:39:58.71	130	367	4.7	224.4	24
Peru	8	2007/08/15 23:40:57.89	63	162	4.7	200	39
Sumatra-Bengkulu	8.5	2007/09/12 11:10:26.83	64	406	4.8	355.7	34
Samoa	8.1	2009/09/29 17:48:10.99	127	306	4.9	224.4	18
Chile	8.8	2010/02/27 06:34:11.53	406	1673	4.7	502.4	23
Japan	9	2011/03/11 05:46:24.12	665	3965	4.7	632.5	29
Total			2763 / 981	11488 /			

Table S2. Event magnitude of completeness

Event Name	M_w	M_c (1 day)	M_c (100 day)
Guam	8	5.0	4.7
Japan-NE	8.1	5.1	4.8
West-Papua	8.2	4.6	4.6
NewIreland-Papua	8	5.2	4.7
Peru-Southern	8.4	5.0	5.0
Hokkaido	8.3	5.2	4.9
Sumatra-Andaman	9	5.0	4.8
Tonga	8	4.9	4.9
Kuril Islands	8.3	4.9	4.8
Solomon Islands	8.1	4.8	4.7
Peru	8	5.0	4.7
Sumatra-Bengkulu	8.5	4.8	4.8
Samoa	8.1	5.0	4.9
Chile	8.8	4.9	4.7
Japan	9	5.1	4.7
Mean	**8.32**	**5.0**	**4.8**
Event Stack Estimated Mc		**5.0**	**4.8**

Table S3. Modified Omori Law parameters for selected events

	M_c	number *	p	c	k	p-err	c-err	k-err	*b* value
Sumatra-Andaman	5**	141/298	2.36	0.544	115.3				1.1
1 day Stack									
	4.9	1207 / 2763	1.04	0.115	518.77	0.16	0.048	28.44	
	5**	980 / 2763	1.04	0.085	373.5	0.15	0.035	23.41	1.13
	5.1	791 / 2763	1.11	0.071	259.1	0.15	0.03	19.43	
100 day Stack									
	4.6	6326 / 11488	1.12	0.342	1357.36	0.01	0.028	55.06	
	4.7**	5135 / 11488	1.13	0.279	1057.71	0.02	0.024	43.76	1.11
	4.8	3991 / 11488	1.15	0.234	806.67	0.02	0.022	35.2	
	4.9	3033 / 11488	1.14	0.159	556.83	0.02	0.017	24.06	
	5	2293 / 11488	1.15	0.122	397.52	0.02	0.015	17.97	
	5.1	1777 / 11488	1.11	0.08	275.82	0.02	0.012	12.45	
Tohoku-Oki 1 day									
	4.2	1021 / 2305	2.7	0.63492	1014.549				0.57
	4.6**	682 / 2305	2.7	0.527	476.1				0.94
	4.7	602 / 2305	2.7	0.49656	374.6059				1.03
Tohoku-Oki 100 day									
	4.6**	1271 / 37882	1.21	0.11	221.63	0.03	0.016	12.6	1.01

* (number at M_c / total aftershocks)
** (used in final results)

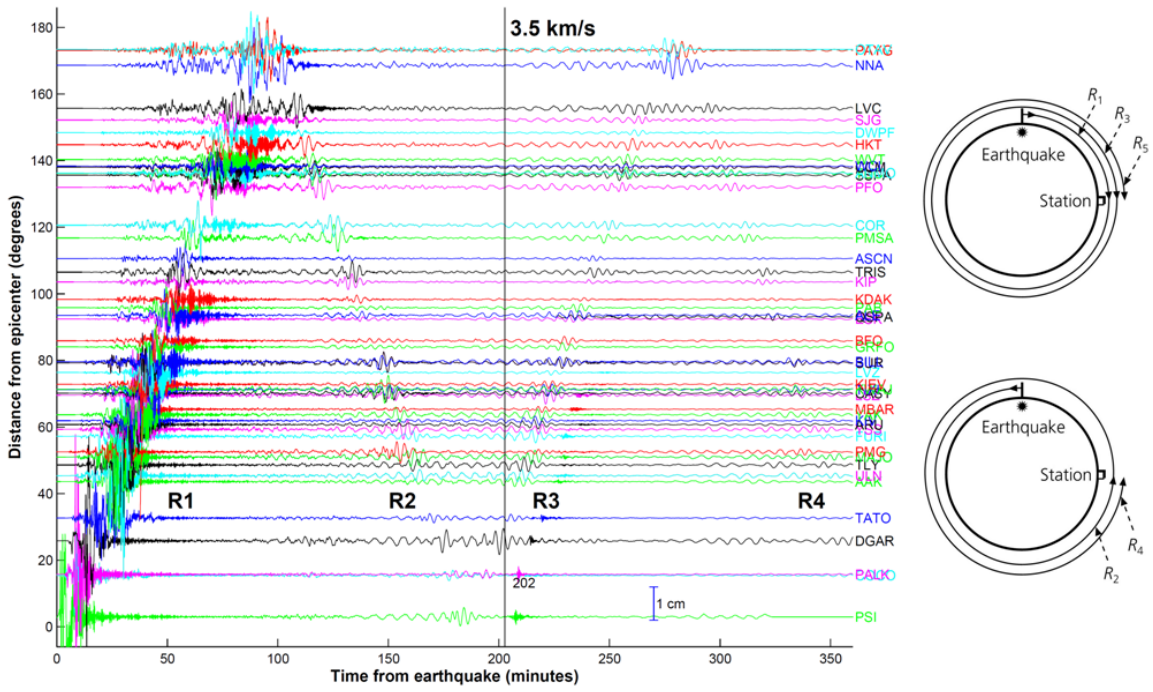

Figure 1. Global displacement wavefield of the December 26, 2004 Sumatra-Andaman Islands Earthquake (Mw=9.0). The Rayleigh surface waves are indicated by R_1-R_4. The magnitude 7.2 aftershock is indicated on the figure at 202 minutes.

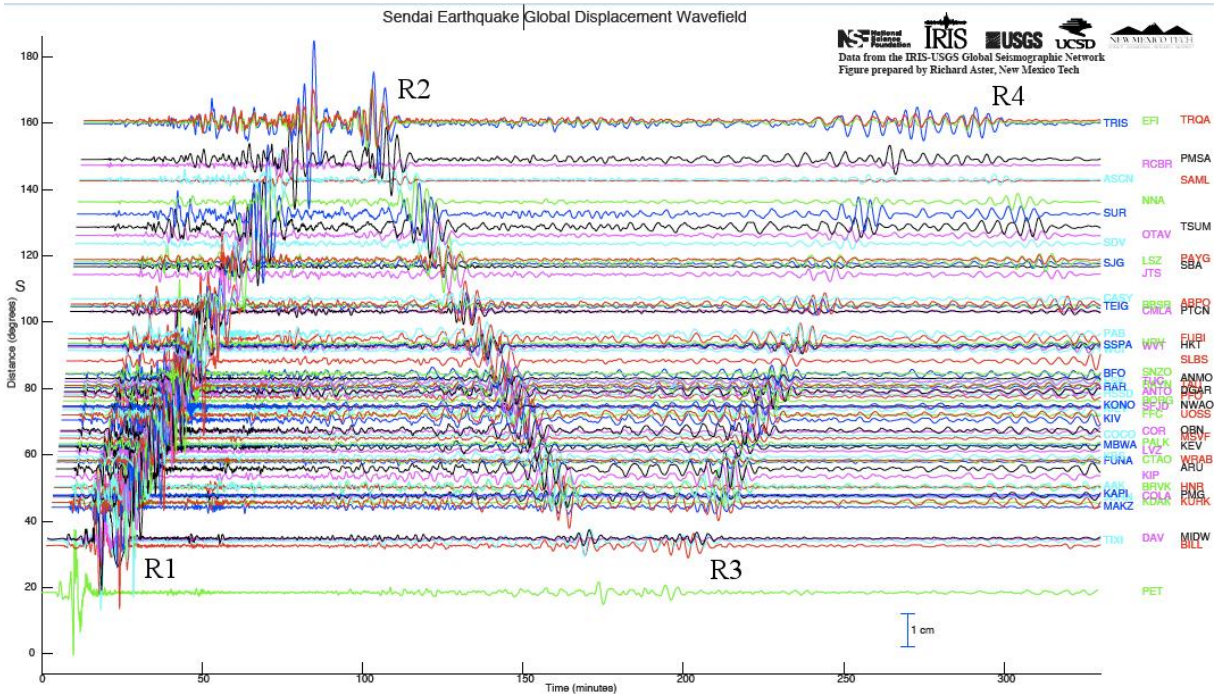

Figure 2. Global displacement wavefield of the March 11, 2011 Tohoku-Oki Earthquake (Mw=9.0). The Rayleigh surface waves are indicated by R_1-R_4 [Courtesy Rick Aster, New Mexico Tech].

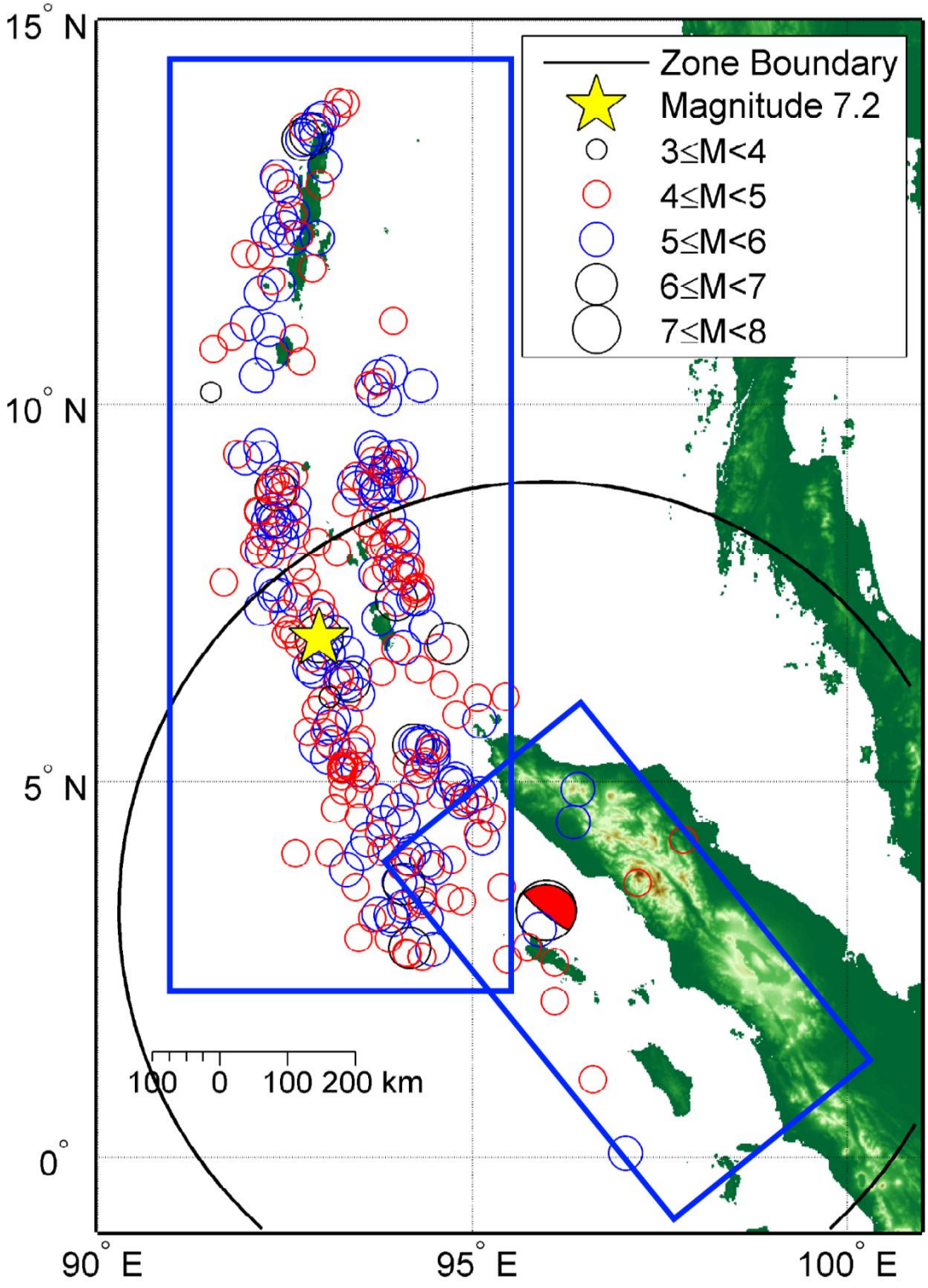

Figure 3. Aftershock zone (24 hour) of the 2004/12/26 M9.0 Sumatra-Andaman Islands Earthquake. Main shock location is given by a red and white beach ball. The black circle indicates the empirically determined Kagan [2002] aftershock region. The modified aftershock zone is shown in blue due to the long rupture length.

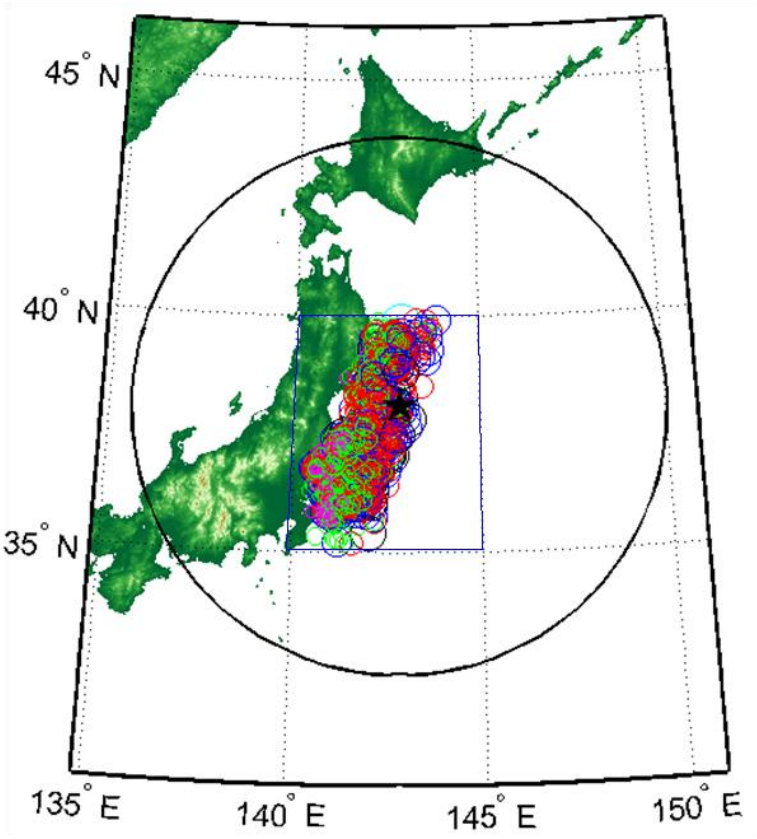

Figure 4. Aftershock zone (24 hour) of the 2011/03/11 M9.0 Tohoku-Oki Earthquake. Main shock location is given by a black star. The black circle indicates the empirically determined Kagan [2002] aftershock region. The modified aftershock zone is given by the blue longitude/latitude bounding box: 140E-145E, and 35N-40N.

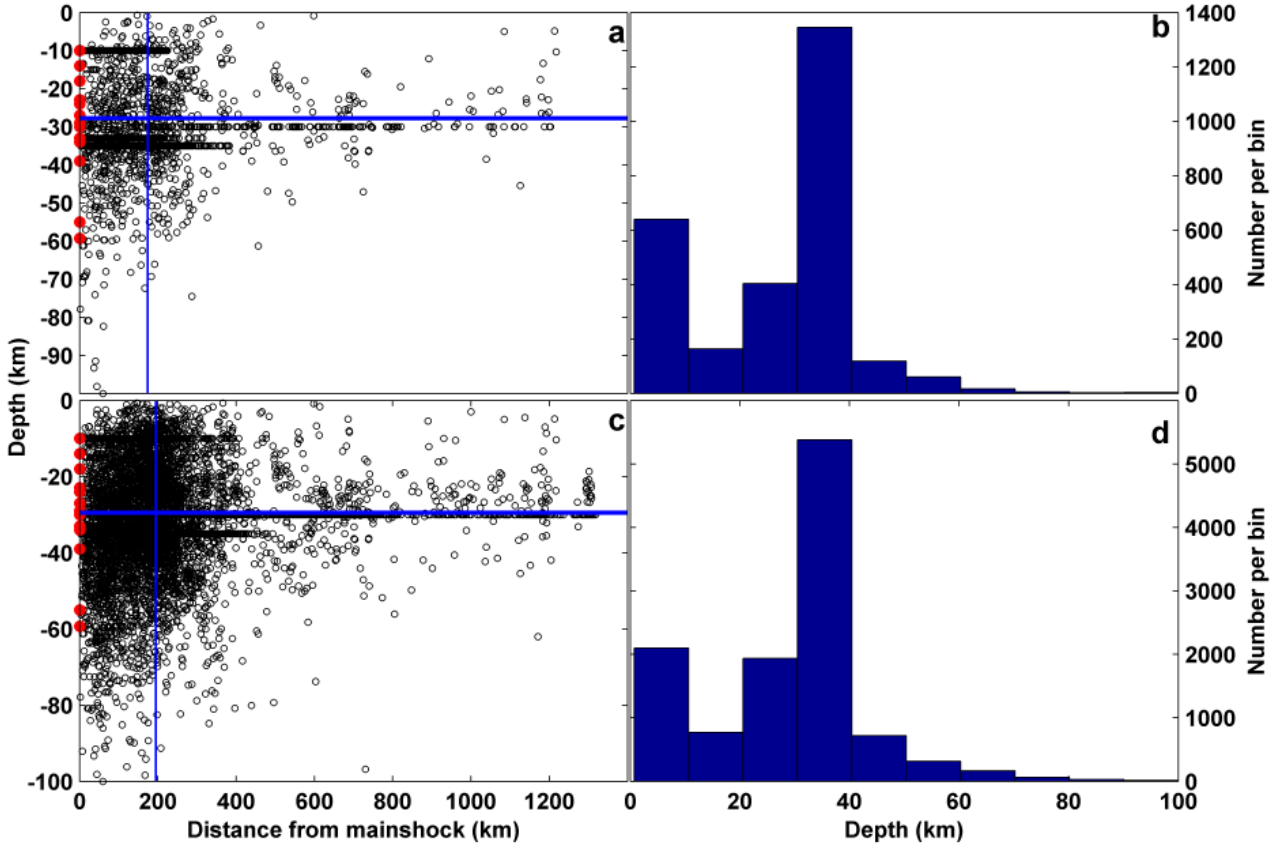

Figure 5. Event stack depth vs. distance from mainshock. (a) Depth vs. distance from mainshock of all 1 day stacked events (b) Depth histogram of all 1 day stacked events (c) Depth vs. distance from mainshock of all 100 day stacked events (d) Depth histogram of all 100 day stacked events. Horizontal and vertical blue lines in (**a, c**) are mean depth and mean distance from mainshock respectively

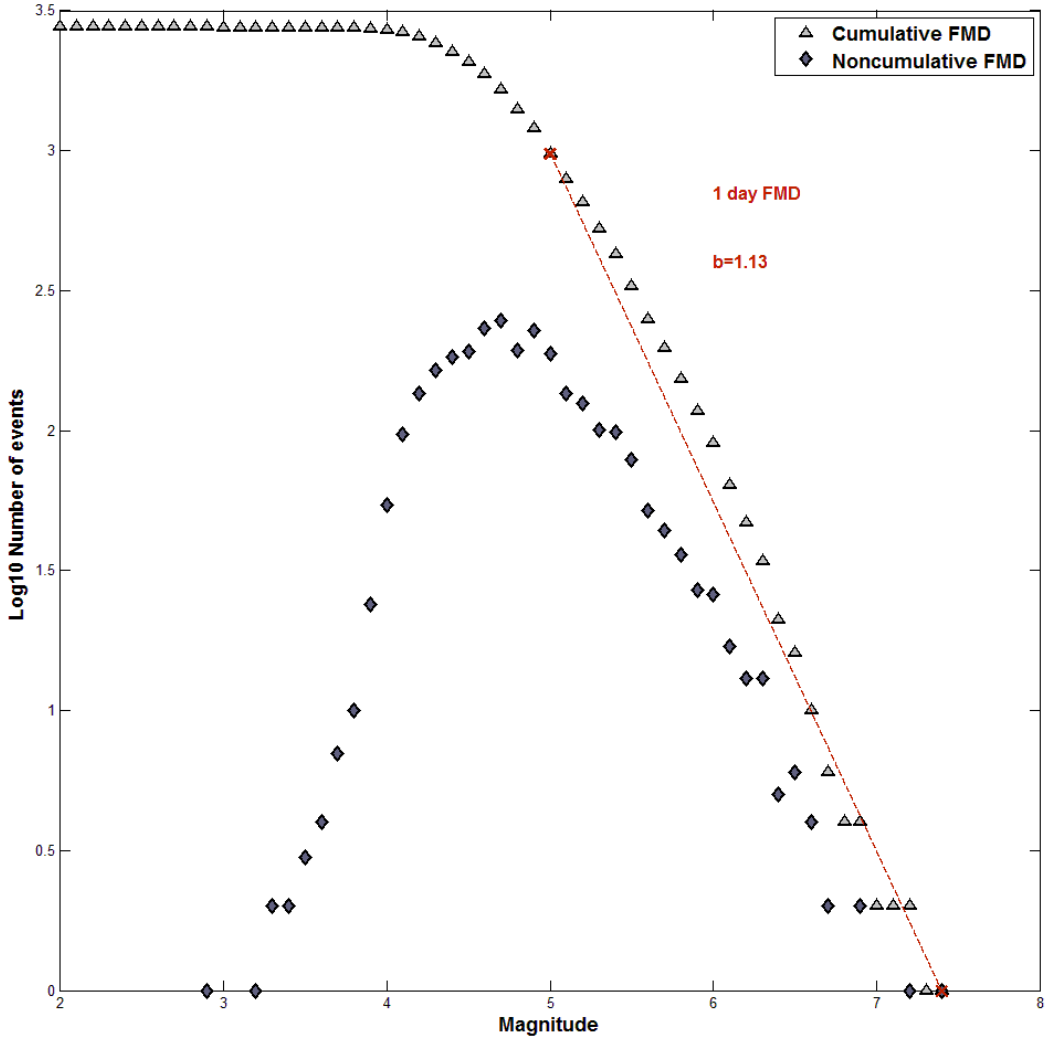

Figure 6. 1 Day Event stack classical Gutenberg-Richter frequency-magnitude plot. Cumulative (triangle) and noncumulative (diamond) number of aftershocks versus magnitude for events listed in the catalog starting right after the mainshock for a 1 day time interval. The dotted red line marks the maximum likelihood fit for the G-R frequency-magnitude relationship. The left red x marks the M_c and start of the fit data. The right red x marks the end of the data used for the fit.

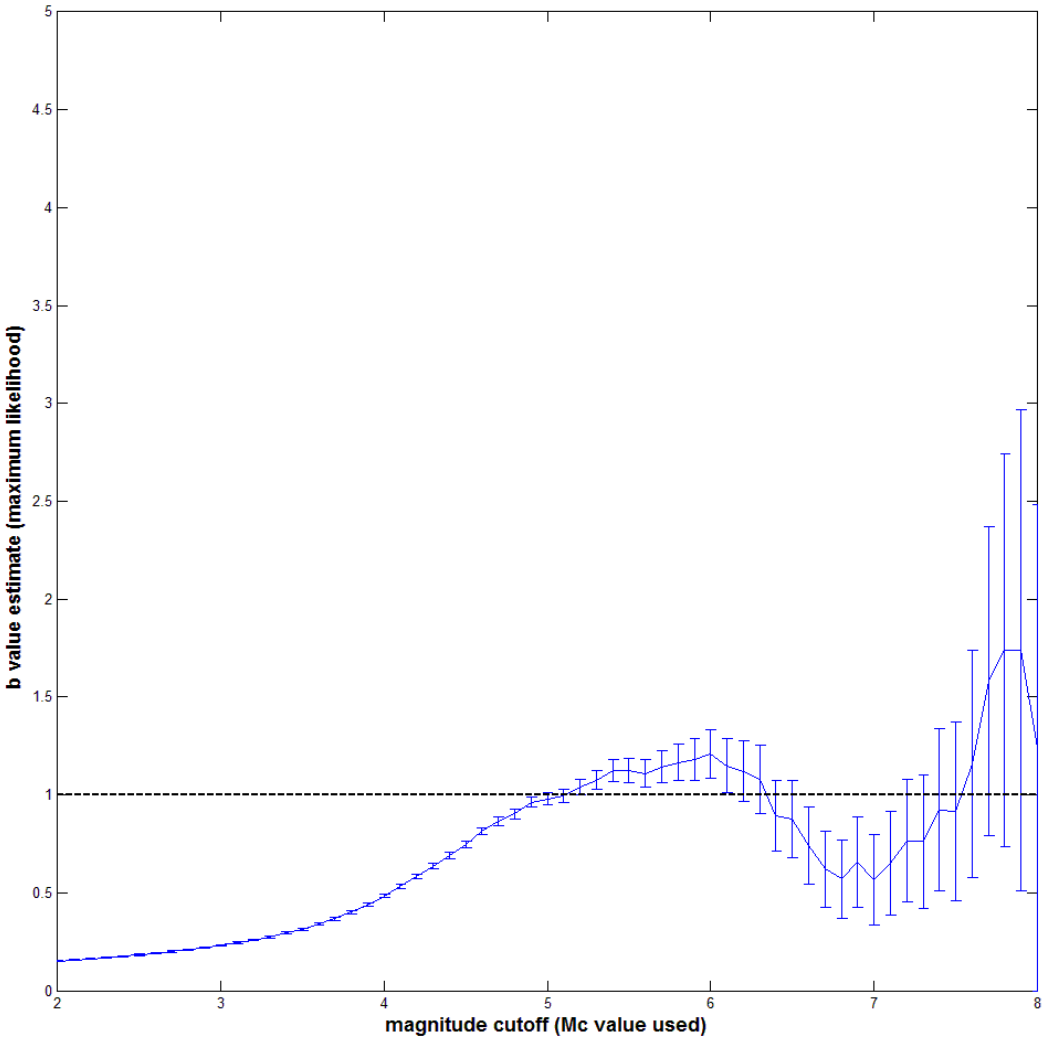

Figure 7. Variation of *b*-value with M_c for the 1 Day Event stack. The black dashed line corresponds to a b-value of 1.

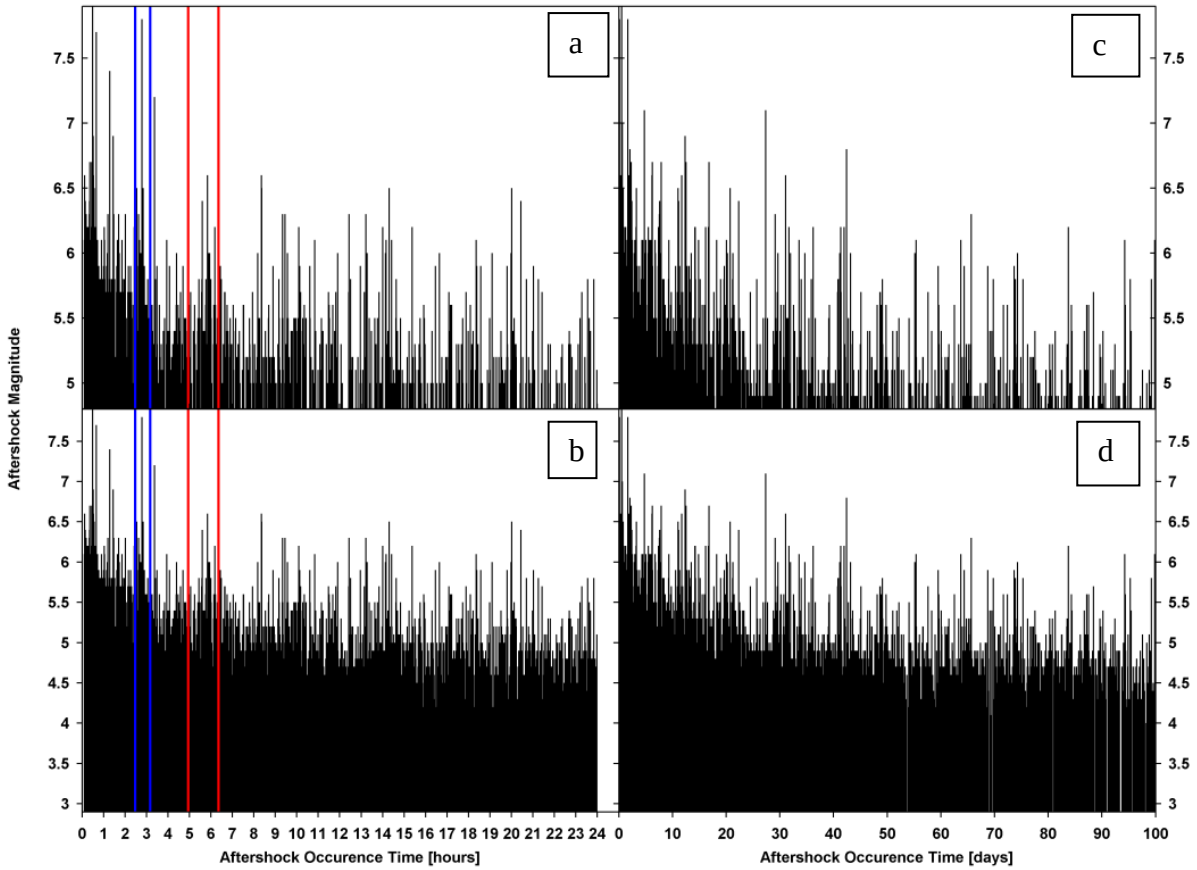

Figure 8. Comb plot of aftershocks. The R_2, R_4 windows are blue, red, respectively. (a) 1 day stack with only the events at M_c (b) 1 day all events (c) 100 day stack with only the events at M_c (d) 100 day all events

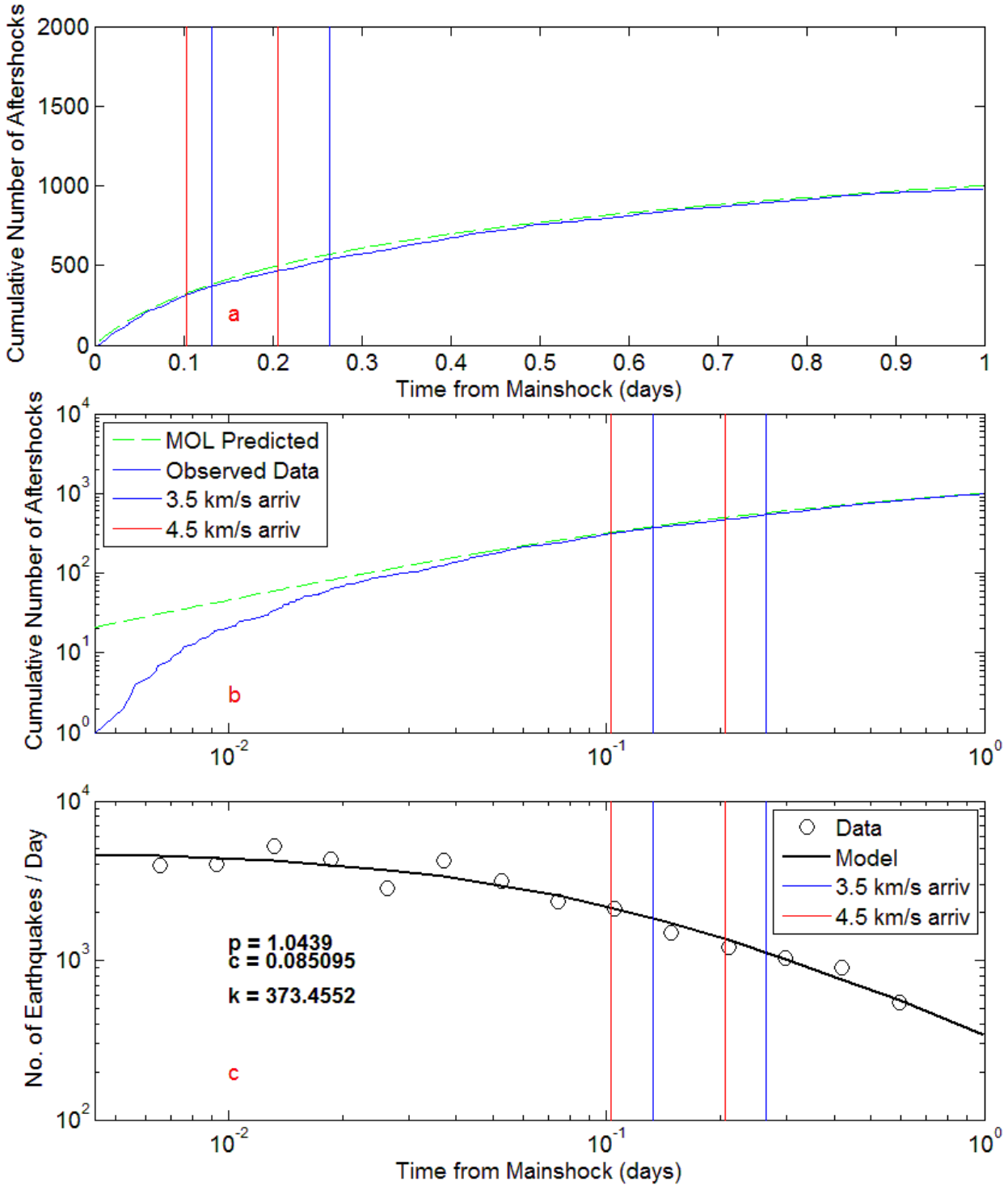

Figure 9. 1 Day Event Stack at M_c of 5.0. (a) Cumulative MOL predicted event numbers vs. observed (b) Log-Log transformed cumulative MOL predicted event numbers vs. observed to emphasize differences at early times. R_2 and R_4 shown as blue and red pairs, respectively. (c) MOL fit plot showing fit versus observed. R_2 and R_4 shown as blue and red pairs, respectively.

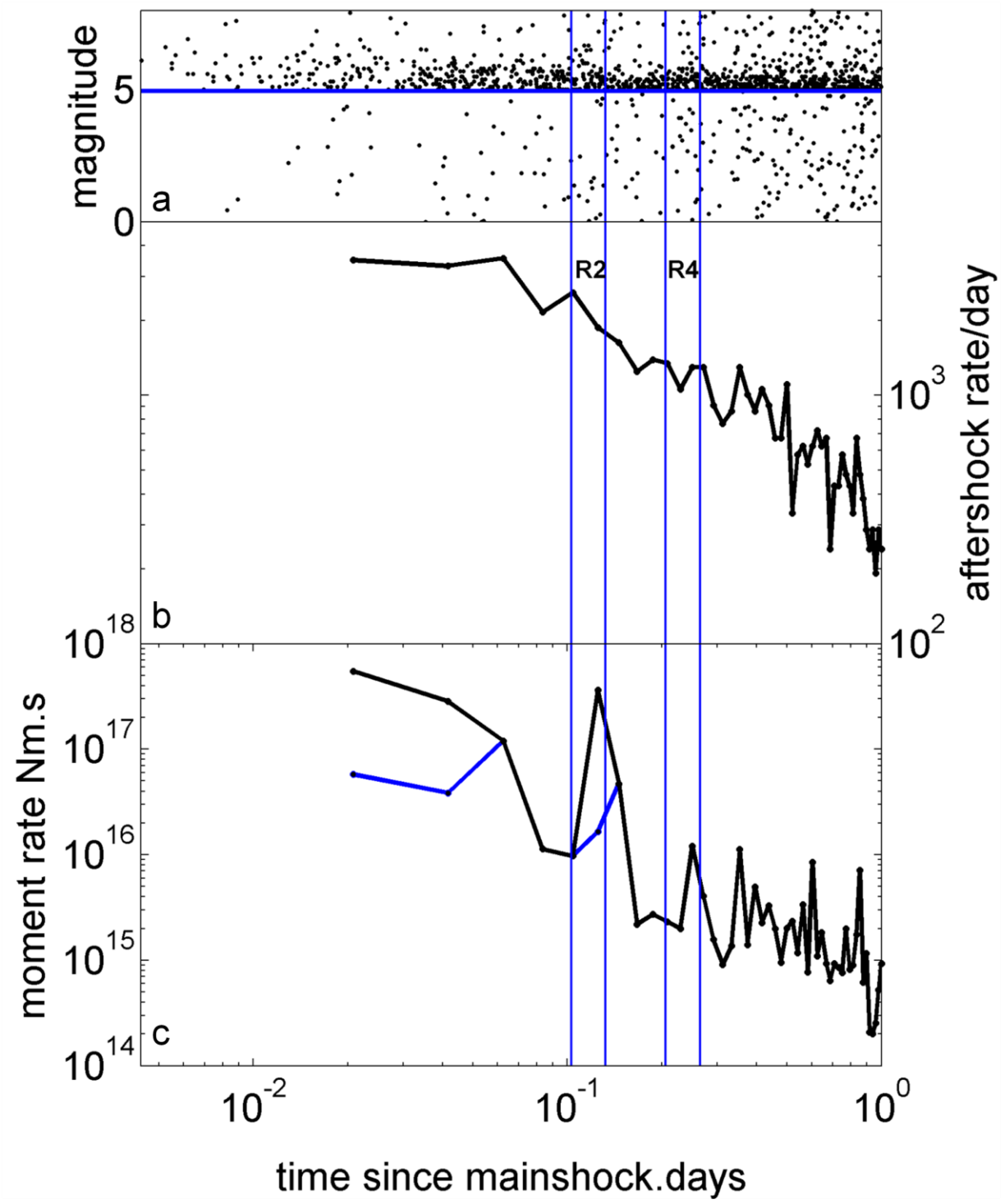

Figure 10. 1 Day Event stack rate calculations for the 15 events. (a) The black circles are the 1 day events. The M_c value (5.0) is shown as a horizontal blue line. Individual sequences had similar M_c. (b) The rate of aftershocks per day for a sliding window of 1800s. The black circles are the estimated rates. (c) The moment rate change is shown in black using all events. The black circles are the estimated rates. The blue line and associated circles uses only events at or below M_w 7.5 in order to lessen the saturation effect of large magnitude events.

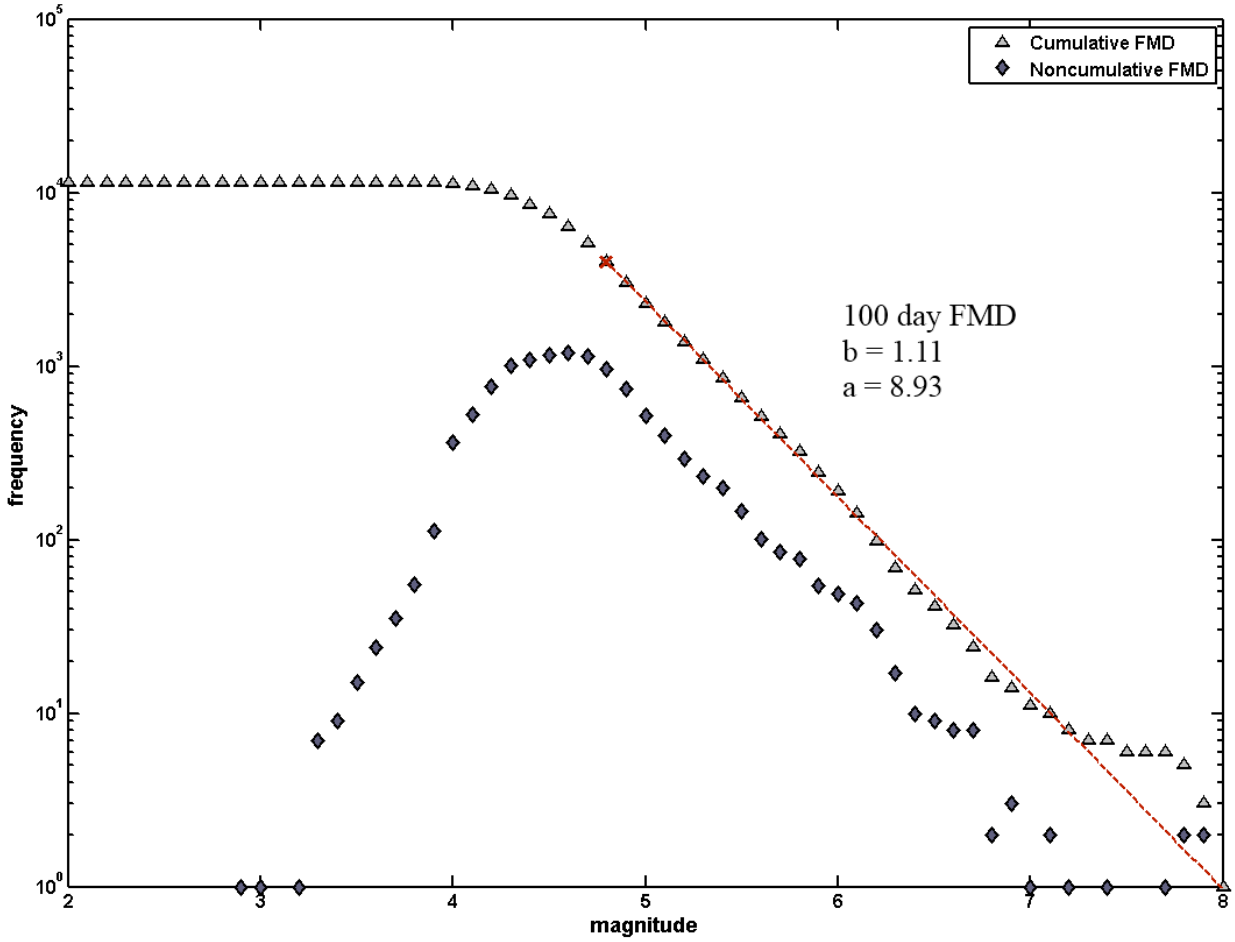

Figure 11. 100 Day Event stack classical Gutenberg-Richter frequency-magnitude plot. Cumulative (triangle) and noncumulative (diamond) number of aftershocks versus magnitude for events listed in the catalog starting right after the mainshock for a 100 day time interval. The dotted red line marks the maximum likelihood fit for the G-R frequency-magnitude relationship. The left red x marks the M_c and start of the fit data. The right red x marks the end of the data used for the fit.

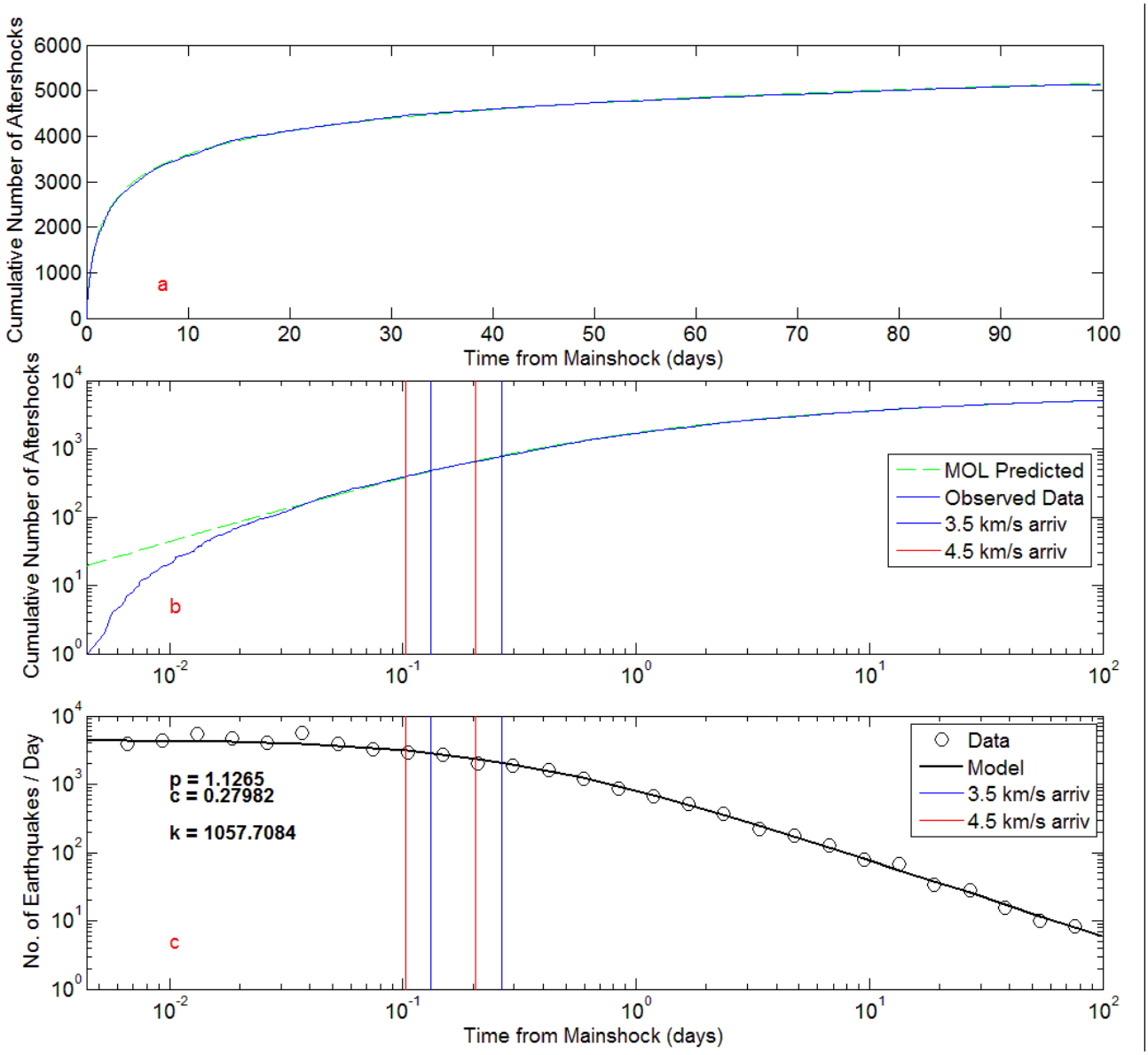

Figure 12. 100 Day Event Stack at M_c=4.7. (a) Plot of cumulative aftershocks from a modified Omori law fit using 5135 events. (b) Transform time plot of cumulative aftershocks versus observed. R_2 and R_4 shown as blue and red pairs, respectively. (c) MOL fit versus observed data. R_2 and R_4 shown as blue and red pairs, respectively.

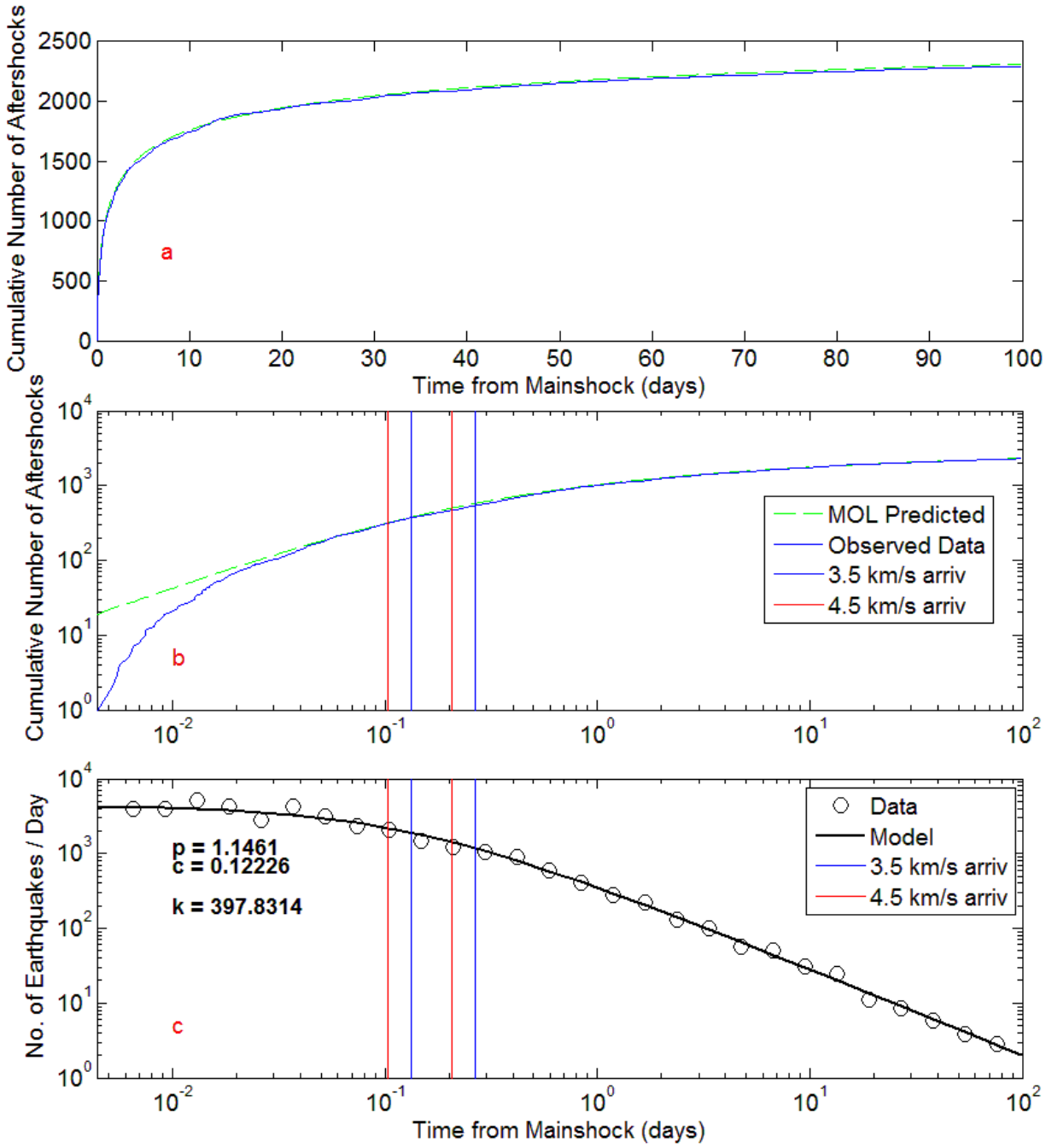

Figure 13. 100 Day Event Stack at M_c=5.0. (a) Plot of cumulative aftershocks from a modified Omori law fit using 2293 events. (b) Transform time plot of cumulative aftershocks versus observed. R_2 and R_4 shown as blue and red pairs, respectively. (c) MOL fit versus observed data. R_2 and R_4 shown as blue and red pairs, respectively.

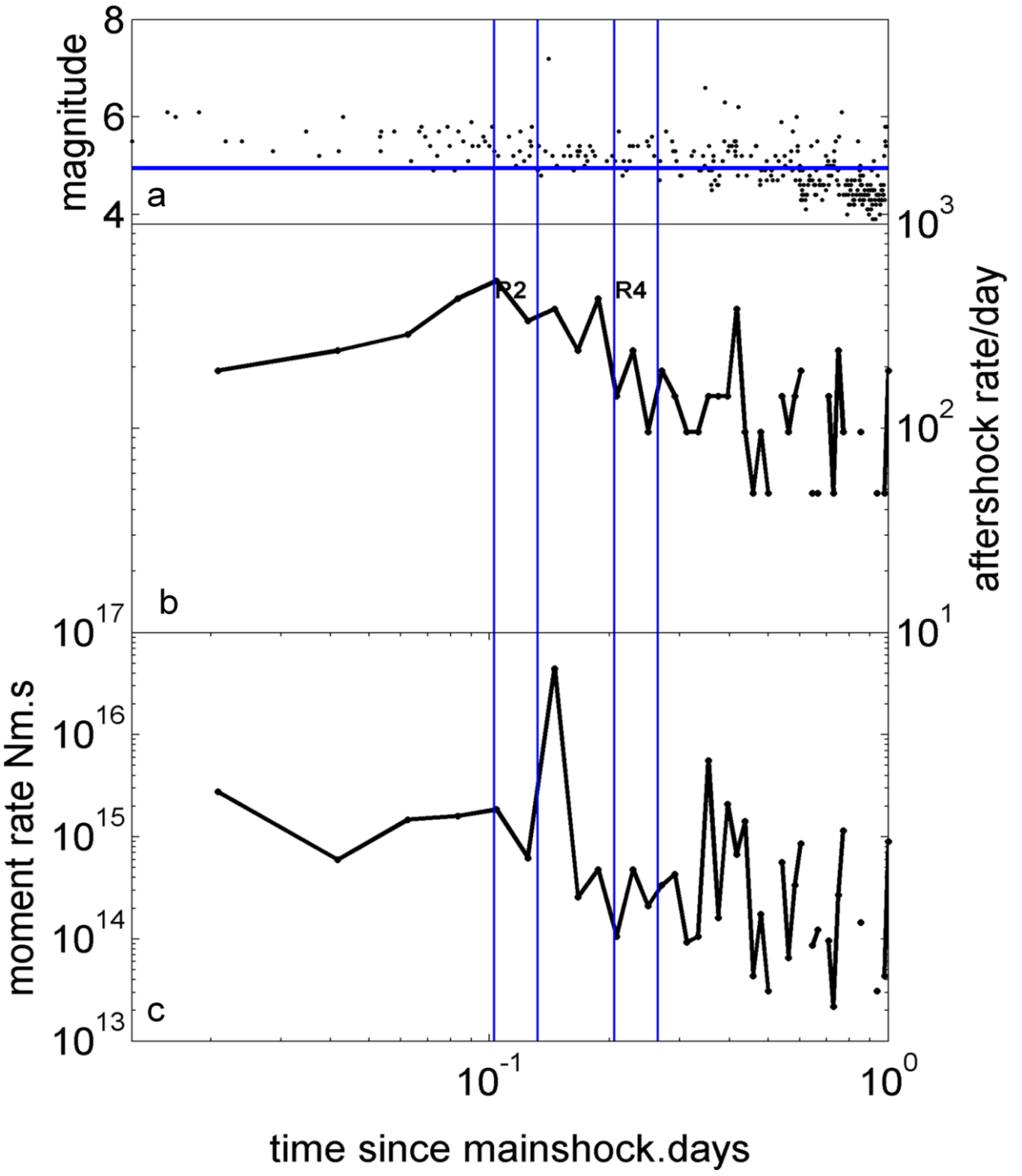

Figure 14. 1 day rate calculations for the Sumatra event. (a) The black circles are the 1 day events. The M_c value of 5.0 is shown as a horizontal blue line at which 141 of 298 aftershocks were above this value. (b) The black circles are the estimated rates. The rate of aftershocks per day for a sliding window of 1800s is plotted. The window size is estimated after the data is cut at the M_c of 5.0. The absolute rates are estimates; however, it is the correlation of arrival times with relative rate changes which is important for this study. The gaps indicate a lack of data during those time windows. (c) The moment rate change is shown using the same technique as above.

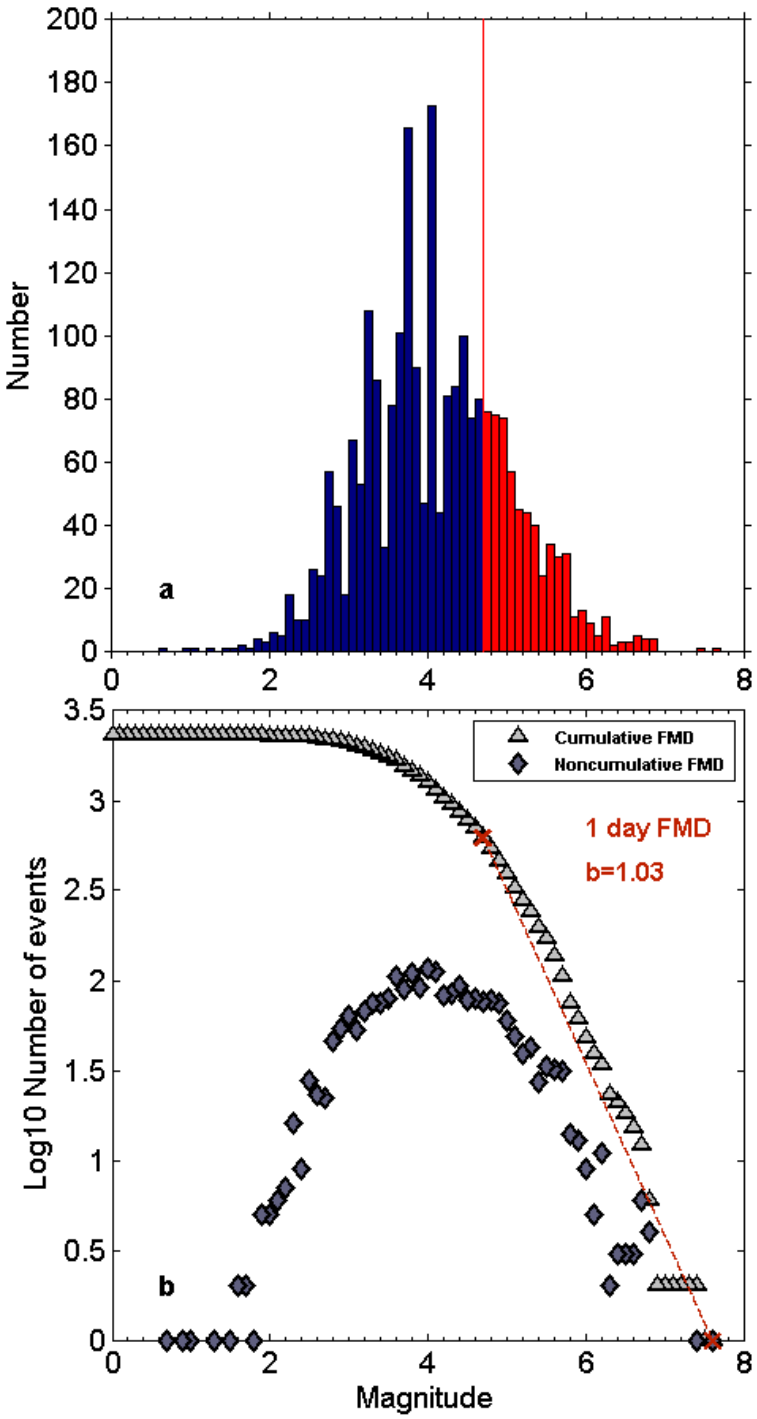

Figure 15. Tohoku-Oki 1 Day, 2305 events. (a) Magnitude histogram showing marked fluctuation from M2.6-M4.6. Blue bars are events below the M_c. Red bars are aftershocks at or above the M_c of 4.7. The red line is placed at the magnitude of 4.7 for reference. (b) G-R plot. Cumulative (triangle) and noncumulative (diamond) number of aftershocks versus magnitude for a 1 day time interval. The dotted red line marks the maximum likelihood fit for the G-R frequency-magnitude relationship. The left red x marks the M_c and start of the fit data. The right red x marks the end of the data used for the fit.

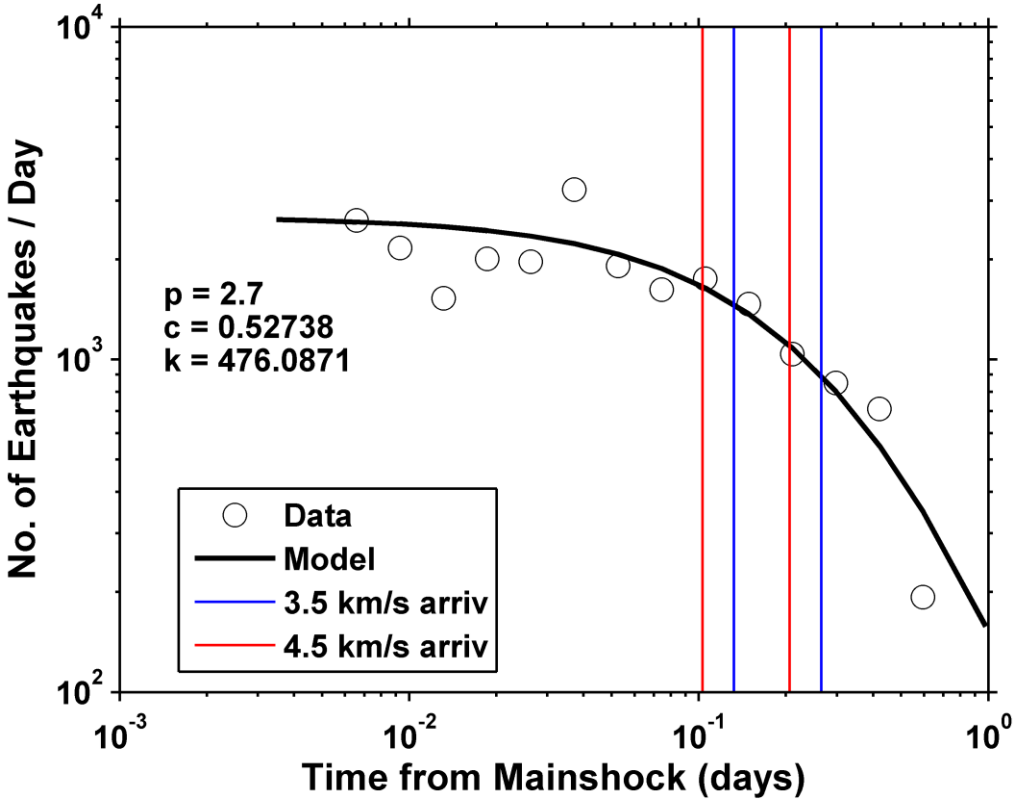

Figure 16. Tohoku-Oki 1 Day. M_c of 4.7, 602 events. MOL fit versus observed data. R_2 and R_4 shown as blue and red pairs, respectively

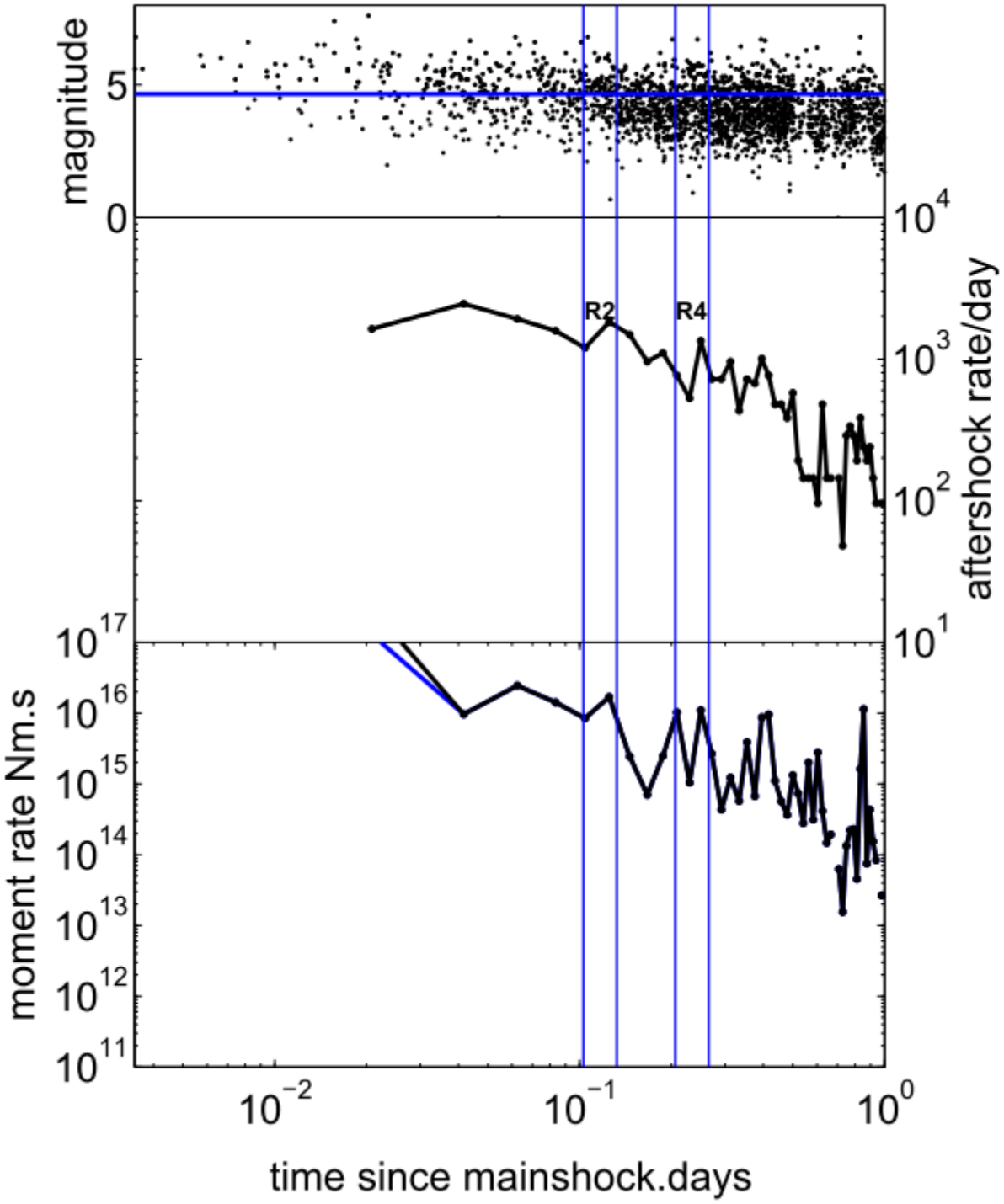

Figure 17. 1 day rate calculations for the Tohoku-Oki event. (a) The black circles are the 1 day events. The M_c of 4.7 is shown as a horizontal blue line at which 377 of 2303 aftershocks were above this value. (b) The black circles are the estimated rates. The rate of aftershocks per day for a sliding window of 1800s. The gaps indicate a lack of data during those time windows. (c) The moment rate change is shown using the same technique as above.

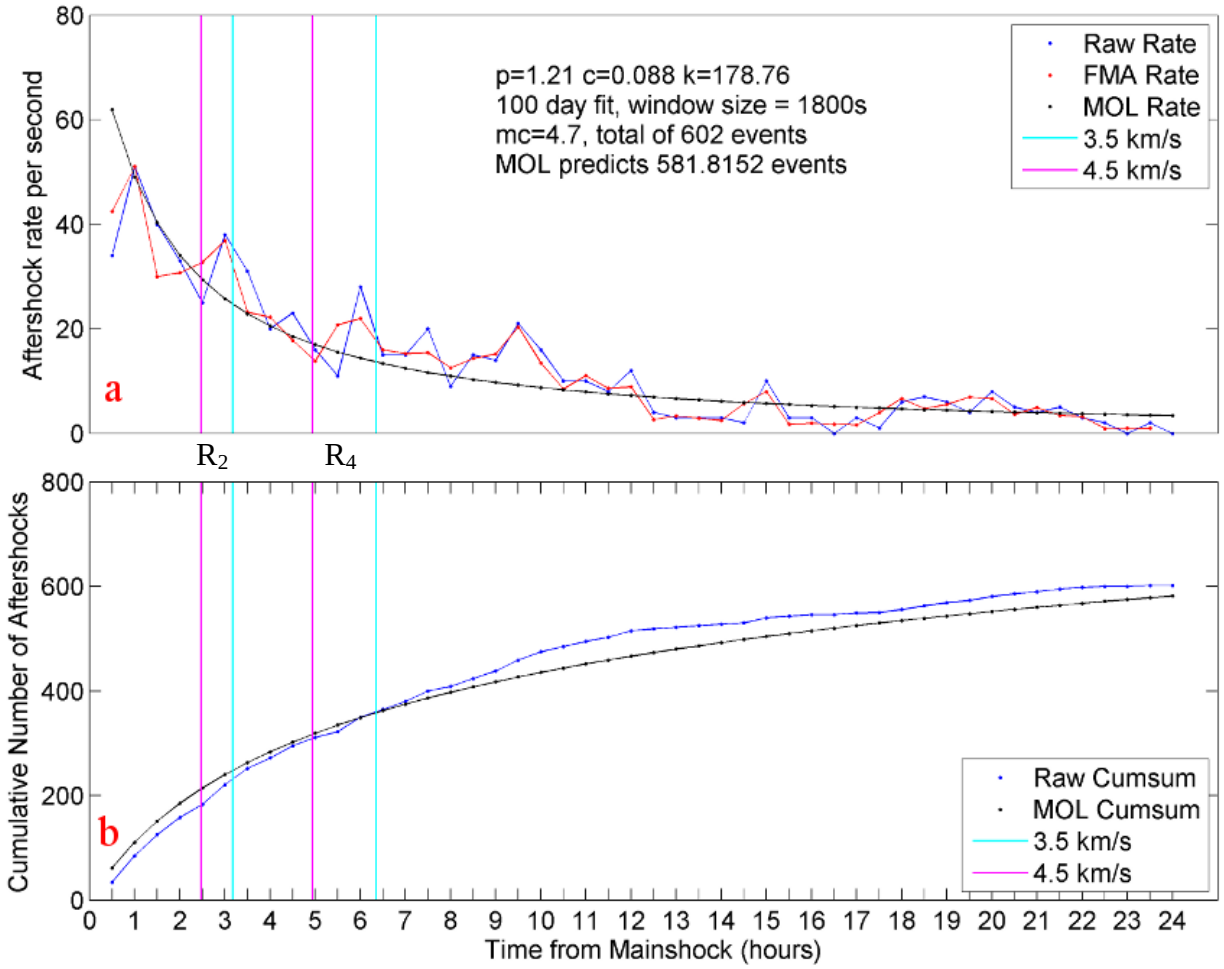

Figure 18. Modified Omori law (MOL) fits 24 hours from the mainshock for the Tohoku-Oki event. The 100 day fit was extrapolated for 1 day. The MOL fit utilized 602 events at a M_c of 4.7. Predicted parameters are p=1.21, c=0.088, and k=178.76. (a) Predicted Omori law rate from 100 day MOL fit with observed rates. The black line indicates the MOL prediction. The red line indicates the observed forward moving average rate and the blue line indicates a simple fixed time window rate. The magenta and cyan lines indicate the R_2 and R_4 arrivals. (b) Cumulative predicated number of aftershocks for the aforementioned MOL parameters versus the observed cumulative number.

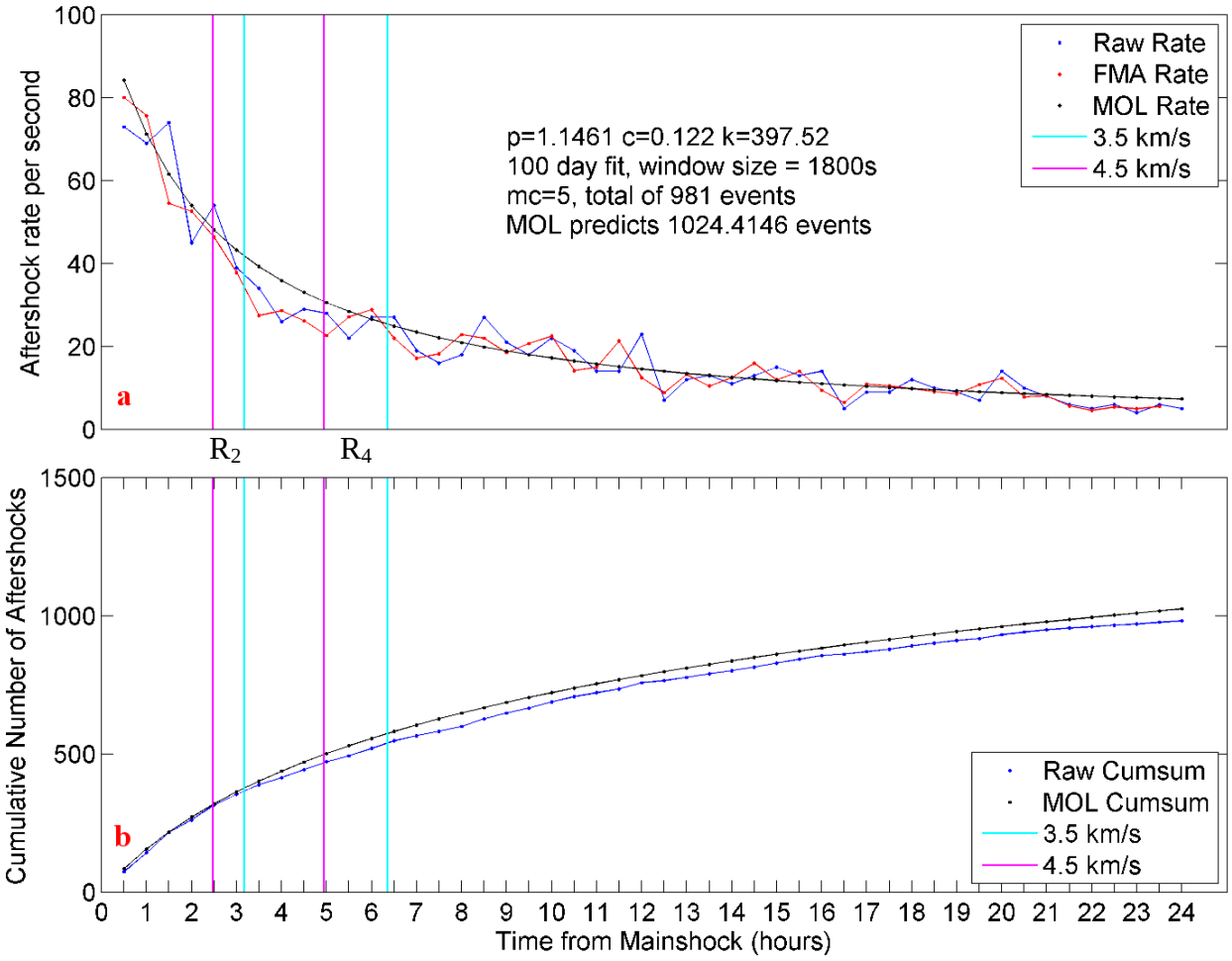

Figure 19. Modified Omori law (MOL) fits for the 15 event stack. The 100 day fit using 2293 events at a M_c of 5.0 was extrapolated to 1 day. Obtained parameters are p=1.14, c=0.122, and k=397.52. (a) Predicted Omori law rate from 100 day MOL fit versus observed 1 day event rates. The black line indicates the MOL prediction. The red line indicates the observed forward moving average rate and the blue line indicates a simple fixed time window rate. The magenta and cyan lines indicate the R_2 and R_4 arrivals. (b) Cumulative predicated number of aftershocks for the aforementioned MOL parameters versus the observed cumulative number.

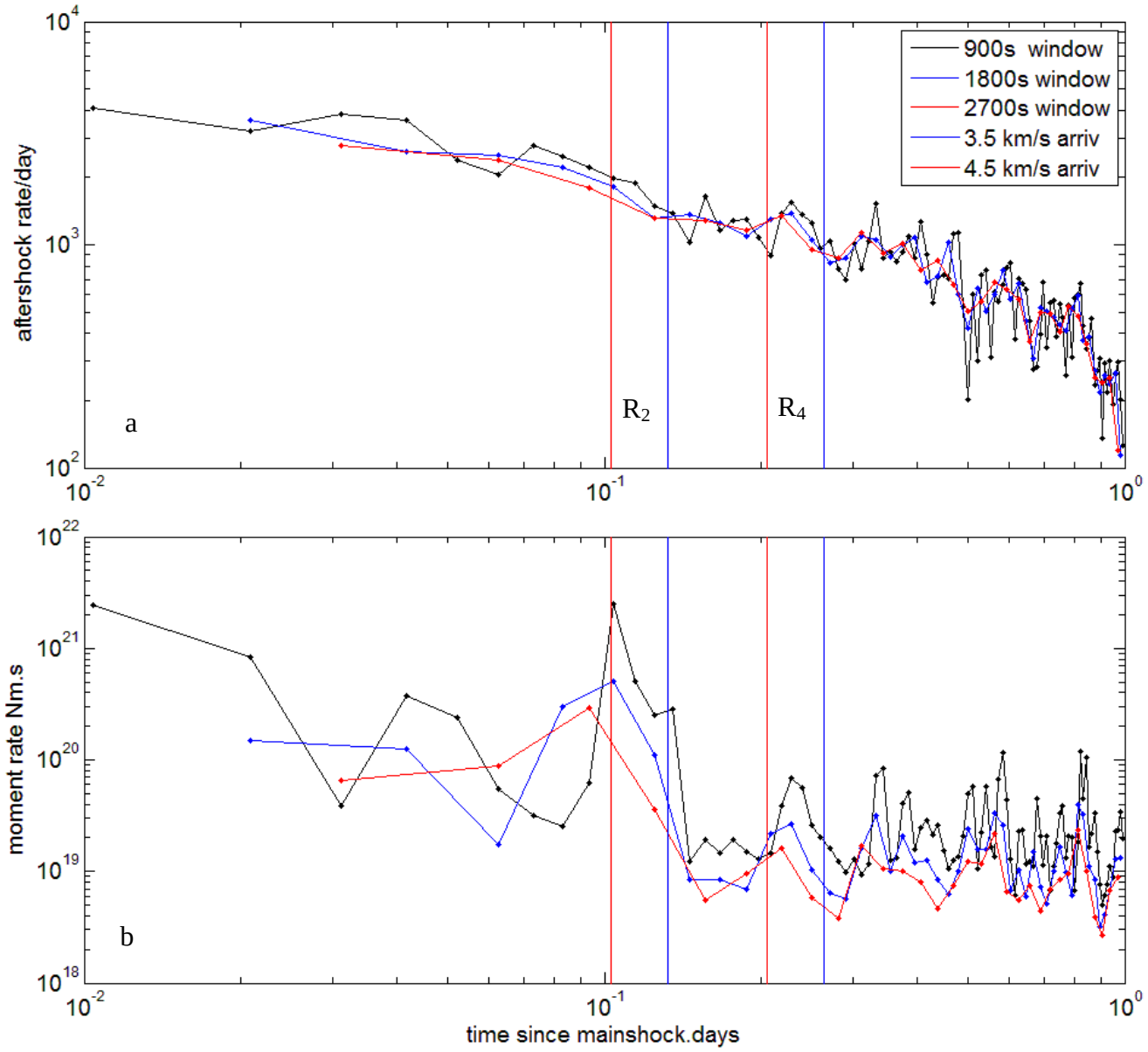

Figure 20. 1 Day Event Stack Rate Comparison at M_c=5.0. (a) Plot of event rate for 3 different time windows (15,30,45 minutes). The R_2 and R_4 arrivals are indicated. (b) Plot of moment rate for the same time windows used in (a).

REFERENCES

Ben-Menahem, A., and S. J. Singh (1981), Seismic Waves and Sources, 2nd ed., Dover Publications Inc., New York.

Ben-Zion, Y., and V. Lyakhovsky (2006), Analysis of aftershocks in a lithospheric model with seismogenic zone governed by damage rheology, Geophysical Journal International, 165(1), 197–210, doi:10.1111/j.1365-246X.2006.02878.x.

Boettcher, M. S., a. McGarr, and M. Johnston (2009), Extension of Gutenberg-Richter distribution to M W -1.3, no lower limit in sight, Geophysical Research Letters, 36(10), 1–5, doi:10.1029/2009GL038080.

Brodsky, E. E., and S. G. Prejean (2005), New constraints on mechanisms of remotely triggered seismicity at Long Valley Caldera, Journal of Geophysical Research, 110(B4), 1–14, doi:10.1029/2004JB003211.

Chao, K., Z. Peng, C. Wu, C.-C. Tang, and C.-H. Lin (2012), Remote triggering of non-volcanic tremor around Taiwan, Geophysical Journal International, 188(1), 301–324, doi:10.1111/j.1365-246X.2011.05261.x.

Davis, S. D., and C. Frohlich (1991), Single-Link Cluster Analysis of Earthquake Aftershocks: Decay Laws and Regional Variations, Journal of Geophysical Research, 96(B4), 6335–6350, doi:10.1029/90JB02634.

Dieterich, J.H. , 1994, A constitutive law for rate of earthquake production and its application to earthquake clustering, J. Geophys. Res. , 99 , 2601-2618.

van der Elst, N. J., and E. E. Brodsky (2010), Connecting near-field and far-field earthquake triggering to dynamic strain, Journal of Geophysical Research, 115(B7), 1–21, doi:10.1029/2009JB006681.

Enescu, B., J. Mori, and M. Miyazawa (2007), Quantifying early aftershock activity of the 2004 mid-Niigata Prefecture earthquake (M w 6.6), Journal of Geophysical Research, 112(B4), doi:10.1029/2006JB004629.

Felzer, K. R., T. W. Becker, R. E. Abercrombie, G. Ekstrom, and J. R. Rice (2002), Triggering of the 1999 M_W 7.1 Hector Mine earthquake by aftershocks of the 1992 M_W 7.3 Landers earthquake, Journal of Geophysical Research, 107(B9), 1–13, doi:10.1029/2001JB000911.

Felzer, K. R. (2012), Stochastic ETAS Aftershock Simulator Program, http://pasadena.wr.usgs.gov/office/kfelzer/AftSimulator.html.

Felzer, K. R., and E. E. Brodsky (2005), Testing the stress shadow hypothesis, Journal of Geophysical Research, 110(B5), 1–13, doi:10.1029/2004JB003277.

Felzer, K. R., and E. E. Brodsky (2006), Decay of aftershock density with distance indicates triggering by dynamic stress., Nature, 441(7094), 735–8, doi:10.1038/nature04799.

Frohlich, C., and S. D. Davis (1993), Teleseismic b Values; Or, Much Ado About 1.0, Journal of Geophysical Research, 98(B1), 631–644, doi:10.1029/92JB01891.

Gonzalez-Huizar, H., A. A. Velasco, Z. Peng, and R. R. Castro (2012), Remote triggered seismicity caused by the 2011, M9.0 Tohoku-Oki, Japan earthquake, Geophysical Research Letters, 39(10), doi:10.1029/2012GL051015.

Guilhem, A., Z. Peng, and R. M. Nadeau (2010), High-frequency identification of non-volcanic tremor triggered by regional earthquakes, Geophysical Research Letters, 37(16), 1–6, doi:10.1029/2010GL044660.

Gutenberg, B., and C. F. Richter (1954), Seismicity of the Earth and Associated Phenomena, Princeton University Press.

Habermann, R. (1988), Precursory seismic quiescence: Past, present, and future, Pure and applied Geophysics, 126(2), 279–318.

Helmstetter, A., and D. Sornette (2002), Subcritical and supercritical regimes in epidemic models of earthquake aftershocks, Journal of Geophysical Research, 107(B10), 1–21, doi:10.1029/2001JB001580.

Helmstetter, A., and D. Sornette (2003), Foreshocks explained by cascades of triggered seismicity, Journal of Geophysical Research, 108(B10), 1–10, doi:10.1029/2003JB002409.

Helmstetter, A., Y. Y. Kagan, and D. D. Jackson (2005), Importance of small earthquakes for stress transfers and earthquake triggering, Journal of Geophysical Research, 110(B5), 1– 13, doi:10.1029/2004JB003286.

Hill, D. P., and S. G. Prejean (2007), 4.09 - Dynamic Triggering, in Treatise on Geophysics, edited by E.-C. G. Schubert, pp. 257–291, Elsevier, Amsterdam.

Hill, D. P. (2010), Surface-Wave Potential for Triggering Tectonic (Nonvolcanic) Tremor, Bulletin of the Seismological Society of America, 100(5A), 1859–1878, doi:10.1785/0120090362.

Holschneider, M., C. Narteau, P. Shebalin, Z. Peng, and D. Schorlemmer (2012), Bayesian analysis of the modified Omori law, Journal of Geophysical Research, 117(B6), 1–12, doi:10.1029/2011JB009054.

Jay, J. A., M. E. Pritchard, M. E. West, D. Christensen, M. Haney, E. Minaya, M. Sunagua, S. R. McNutt, M. Zabala (2012) Shallow seismicity, triggered seismicity, and ambient noise tomography at the long-dormant Uturuncu volcano, Bolivia, Bulletin of Volcanology, Bull. Volcano., 74(4), 817-837.

Kagan, Y. Y. (2002), Aftershock Zone Scaling, Bulletin of the Seismological Society of America, 92(2), 641–655, doi:10.1785/0120010172.

Kagan, Y. Y. (2004), Short-Term Properties of Earthquake Catalogs and Models of Earthquake Source, Bulletin of the Seismological Society of America, 94(4), 1207–1228, doi:10.1785/012003098.

Kagan, Y. Y., and H. Houston (2005), Relation between mainshock rupture process and Omori's law for aftershock moment release rate, Geophysical Journal International, 163(3), 1039–1048, doi:10.1111/j.1365-246X.2005.02772.x.

Kagan, Y. Y. (2010), Earthquake size distribution: Power-law with exponent ?, Tectonophysics, 490(1-2), 103–114, doi:10.1016/j.tecto.2010.04.034.

Kanamori, H., and E. E. Brodsky (2004), The physics of earthquakes, Reports on Progress in Physics, 67(8), 1429–1496, doi:10.1088/0034-4885/67/8/R03.

King, G. C. P., R. S. Stein, and J. Lin (1995), Static stress changes and the triggering of earthquakes, Bulletin of the Seismological Society of America, 32(2), A50–A51, doi:10.1016/0148-9062(95)94484-2.

Lay, T. et al. (2005), The great Sumatra-Andaman earthquake of 26 December 2004., Science (New York, N.Y.), 308(5725), 1127–33, doi:10.1126/science.1112250.

Lengliné, O., B. Enescu, Z. Peng, and K. Shiomi (2012), Decay and expansion of the early aftershock activity following the 2011, Mw9.0 Tohoku earthquake, Geophys. Res. Lett., doi:10.1029/2012GL052797, in press.

Lin, C. (2010), A Large Mw 6.0 Aftershock of the 2008 Mw 7.9 Wenchuan Earthquake Triggered by Shear Waves Reflected from the Earth's Core, Bulletin of the Seismological Society of America, 100(5B), 2858–2865, doi:10.1785/0120090141.

Lin, C. (2012), Remote Triggering of the M w 6 . 9 Hokkaido Earthquake as a Result of the M w 6 . 6 Indonesian Earthquake on September 11 , 2008, Terrestrial, Atmospheric and Oceanic Sciences, 23(3), 283–290, doi:10.3319/TAO.2012.01.12.01(T)1.

Marzocchi, W., and L. Sandri (2003), A review and new insights on the estimation of the b-value and its uncertainty, Annals of geophysics, 46(December).

Matthews, M. V., and P. A. Reasenberg (1988), Statistical methods for investigating quiescence and other temporal seismicity patterns, Pure and Applied Geophysics, 126(2-4), 357-372.

Meng, X., X. Yu, Z. Peng, and B. Hong (2012), Detecting Earthquakes around Salton Sea Following the 2010 Mw7.2 El Mayor-Cucapah Earthquake Using GPU Parallel Computing, Procedia Computer Science, 9, 937–946, doi:10.1016/j.procs.2012.04.100.

Miyazawa, M. (2011), Propagation of an earthquake triggering front from the 2011 Tohoku- Oki earthquake, Geophysical Research Letters, 38(23), 1–7, doi:10.1029/2011GL049795.

Miyazawa, M., and J. Mori (2006), Evidence suggesting fluid flow beneath Japan due to periodic seismic triggering from the 2004 Sumatra-Andaman earthquake, Geophysical Research Letters, 33(5), 2–5, doi:10.1029/2005GL025087.

Nyffenegger, P., and C. Frohlich (1998), Recommendations for Determining p Values for Aflershock Sequences and Catalogs, Bulletin of the Seismological Society of America, 88(5), 1144–1154.

Ogata, Y., and K. Shimazaki (1984), Transition from aftershock to normal activity: the 1965 Rat Islands earthquake aftershock sequence, Bulletin of the Seismological Society of America, 74(5), 1757.

Ogata, Y. (1988), Statistical models for earthquake occurrences and residual analysis for point processes, Journal of the American Statistical Association, 83(401), 9–27.

Ogata, Y. (1998), Space-Time Point-Process Models for Earthquake Occurrences, Annals of the Institute of Statistical Mathematics, 50(2), 379–402, doi:10.1023/A:1003403601725.

Ogata, Y. (2006), Statistical analysis of seismicity, Computer Science Monographs, 79(4), 973.

Okal, E. A., and B. A. Romanowicz (1994), On the variation of b-values with earthquake size, Physics of the Earth and Planetary Interiors, 87(1-2), 55–76, doi:10.1016/0031-9201(94)90021-3.

Omori, F. (1894), On the after-shocks of earthquakes, Journal of the College of Science, Imperial University of Tokyo, 7, 111-200.

Parsons, T. (2005), A hypothesis for delayed dynamic earthquake triggering, Geophys. Res. Lett., 32, L04302, doi:10.1029/2004GL021811.

Parsons, T., and A. a. Velasco (2011), Absence of remotely triggered large earthquakes beyond the mainshock region, Nature Geoscience, 4(5), 312–316, doi:10.1038/ngeo1110.

Peng, Z., and J. Gomberg (2010), An integrated perspective of the continuum between earthquakes and slow-slip phenomena, Nature Geoscience, 3(9), 599–607, doi:10.1038/ngeo940.

Peng, Z., D. Hill, D. Shelly and C. Aiken (2010), Remotely triggered microearthquakes and tremor in Central California following the 2010 M_w 8.8 Chile Earthquake, Geophys. Res. Lett., 37, L24312, doi:10.1029/2010GL045462.

Peng, Z., J. E. Vidale, and H. Houston (2006), Anomalous early aftershock decay rate of the 2004 Mw6.0 Parkfield, California, earthquake, Geophysical Research Letters, 33(17), doi:10.1029/2006GL026744.

Peng, Z., J. E. Vidale, M. Ishii, and A. Helmstetter (2007), Seismicity rate immediately before and after main shock rupture from high-frequency waveforms in Japan, Journal of Geophysical Research, 112(B3), 1–15, doi:10.1029/2006JB004386.

Peng, Z., J. E. Vidale, A. G. Wech, R. M. Nadeau, and K. C. Creager (2009), Remote triggering of tremor along the San Andreas Fault in central California, Journal of Geophysical Research, 114, 1–18, doi:10.1029/2008JB006049.

Peng, Z., W. Wang, Q. Chen, and T. Jiang (2011a), Remotely triggered seismicity in north China following the 2008 M w 7.9 Wenchuan earthquake, Earth, Planets and Space, 62(11), 893–898, doi:10.5047/eps.2009.03.006.

Peng, Z., C. Wu, and C. Aiken (2011b), Delayed triggering of microearthquakes by multiple surface waves circling the Earth, Geophysical Research Letters, 38(4), 1–5, doi:10.1029/2010GL046373.

Peng, Z., and P. Zhao (2009), Migration of early aftershocks following the 2004 Parkfield earthquake, Nature Geoscience, 2(12), 877–881, doi:10.1038/ngeo697.

Pollitz, F. F., R. S. Stein, and Roland Burgmann (2012), The 11 April 2012 M=8.6 East Indian Ocean earthquake triggered large aftershocks worldwide, Nature, in review.

Reasenberg, P. A, and L. M. Jones (1989), Earthquake hazard after a mainshock in California., Science (New York, N.Y.), 243(4895), 1173–6, doi:10.1126/science.243.4895.1173.

Rial, J. A., and V. F. Cormier (1980), Seismic waves at the epicenter's antipode, Journal of Geophysical Research, 85(80), 2661–2668.

Romanowicz, B. (2002), Inversion of Surface Waves: A Review, in International Handbook of Earthquake and Engineering Seismology, vol. 81, edited by W. H. K. Lee, H. Kanamori, P. Jennings, and C. Kisslinger, pp. 149–173, Academic Press, Amsterdam.

Sato, H., and M. C. Fehler (2009), Seismic Wave Propagation and Scattering in the Heterogeneous Earth, Springer Berlin Heidelberg, Berlin, Heidelberg.

Shelly, D. R., G. C. Beroza, and S. Ide (2007), Non-volcanic tremor and low-frequency earthquake swarms., Nature, 446(7133), 305–7, doi:10.1038/nature05666.

van Stiphout, T., D. Schorlemmer, and S. Wiemer (2011), The Effect of Uncertainties on Estimates of Background Seismicity Rate, Bulletin of the Seismological Society of America, 101(2), 482–494, doi:10.1785/0120090143.

Tosi, P., V. Rubeis, and P. Sbarra (2010), Stacked Analysis of Earthquake Sequences: Statistical Space–Time Definition of Clustering and Omori Law Behavior, in Synchronization and Triggering: from Fracture to Earthquake Processes, vol. 1, edited by V. Rubeis, Z. Czechowski, and R. Teisseyre, pp. 323–337, Springer Berlin Heidelberg.

Utsu, T. (1961), A statistical study of the occurrence of aftershocks, Geophysical Magazine, 30, 521–605.

Utsu, T., Y. Ogata, and R. Matsu'ura (1995), The centenary of the Omori formula for a decay law of aftershock activity, Journal of Physics of the Earth, 43(1), 1–33.

Wang, Q., F. P. Schoenberg, and D. D. Jackson (2010), Standard Errors of Parameter Estimates in the ETAS Model, Bulletin of the Seismological Society of America, 100(5A), 1989–2001, doi:10.1785/0120100001.

West, M., J. J. Sánchez, and S. R. McNutt (2005), Periodically triggered seismicity at Mount Wrangell, Alaska, after the Sumatra earthquake., Science (New York, N.Y.), 308(5725), 1144–6, doi:10.1126/science.1112462.

Wiemer, S., and M. Wyss (2000), Minimum Magnitude of Completeness in Earthquake Catalogs: Examples from Alaska, the Western United States, and Japan, Bulletin of the Seismological Society of America, 90(4), 859–869, doi:10.1785/0119990114.

Wiemer, S. (2001), A Software Package to Analyze Seismicity: ZMAP, Seismological Research Letters, 72, 373–382.

Woessner, J., and S. Wiemer (2005), Assessing the Quality of Earthquake Catalogues: Estimating the Magnitude of Completeness and Its Uncertainty, Bulletin of the Seismological Society of America, 95(2), 684–698, doi:10.1785/0120040007.

Woessner, J., J. Hardebeck, and E. Hauksson (2010), What is an instrumental seismicity catalog?, in Understanding Seismicity Catalogs and their Problems, pp. 1–14.

Wu, C., Z. Peng, W. Wang, and Q.-F. Chen (2011), Dynamic triggering of shallow earthquakes near Beijing, China, Geophysical Journal International, 185(3), 1321–1334, doi:10.1111/j.1365-246X.2011.05002.x.

Zaliapin, I., A. Gabrielov, V. Keilis-Borok, and H. Wong (2008), Clustering Analysis of Seismicity and Aftershock Identification, Physical Review Letters, 101(1), 4–7, doi:10.1103/PhysRevLett.101.018501.

Zigone, D., D. Rivet, M. Radiguet, M. Campillo, C. Voisin, N. Cotte, A. Walpersdorf, N. M. Shapiro, G. Cougoulat, P. Roux, V. Kostoglodov, A. L. Husker, and J. S. Payero (2012), Triggering of Tremors and Slow Slip event in Guerrero (Mexico) by the 2010 Mw 8.8 Maule, Chile, Earthquake, J. Geophys. Res., doi:10.1029/2012JB009160,in press.